RECEIVED BY OSTI JAN 22 1986

LBL-20627

Lawrence Berkeley Laboratory
UNIVERSITY OF CALIFORNIA

Engineering Division

TRANSIENT AND TEMPERATURE-DEPENDENT PHENOMENA IN Ge:Be AND Ge:Zn FAR INFRARED PHOTOCONDUCTORS

N.M. Haegel
(Ph.D. Thesis)

November 1985

Prepared for the U.S. Department of Energy under Contract DE-AC03-76SF00098

LBL--20627

DE86 005191

TRANSIENT AND TEMPERATURE-DEPENDENT PHENOMENA IN Ge:Be and Ge:Zn FAR INFRARED PHOTOCONDUCTORS

Nancy Marie Haegel
(Ph.D. Thesis)

Lawrence Berkeley Laboratory
University of California
Berkeley, California 94720

November 1985

DISCLAIMER

This report was prepared as an account of work sponsored by an agency of the United States Government. Neither the United States Government nor any agency thereof, nor any of their employees, makes any warranty, express or implied, or assumes any legal liability or responsibility for the accuracy, completeness, or usefulness of any information, apparatus, product, or process disclosed, or represents that its use would not infringe privately owned rights. Reference herein to any specific commercial product, process, or service by trade name, trademark, manufacturer, or otherwise does not necessarily constitute or imply its endorsement, recommendation, or favoring by the United States Government or any agency thereof. The views and opinions of authors expressed herein do not necessarily state or reflect those of the United States Government or any agency thereof.

MASTER

ABSTRACT

An experimental study of the transient and temperature-dependent behavior of Ge:Be and Ge:Zn photoconductors has been performed under the low background photon flux conditions ($\dot{p}\approx10^8$ photons/second) typical of astronomy and astrophysics applications. Ge:Be and Ge:Zn single crystals were grown using a high purity Czochralski crystal grower to achieve good control of residual impurity concentrations. The responsivity of Ge:Be and Ge:Zn detectors is strongly temperature-dependent in closely compensated material, and the effect of compensation on free carrier lifetime in Ge:Be has been measured using the photo-Hall effect technique. Closely compensated material has been obtained by controlling the concentration of novel hydrogen-related shallow acceptor complexes, A(Be,H) and A(Zn,H), which exist in doped crystals grown under a H_2 atmosphere. A review of selection criteria for multilevel materials for optimum photoconductor performance is included.

Transient behavior with respect to changes in incident photon flux levels has been observed to occur in both Ge:Be and Ge:Zn photoconductors with time constants ranging from 0.1 to greater than 5.0 seconds. The detector response consists of both a fast and a slow component. The amplitude of the slow component can be up to ten times greater than the initial fast component. It has been established that this phenomena cannot be explained by current models of carrier sweep-out and dielectric relaxation. This transient behavior has been characterized as a function of temperature, electric field, contact area, photoconductive gain, and material parameters. The time constant of the slow response decreases

with increasing temperature, but is found to be independent of electric field, background photon flux, and photoconductive gain. Transient solutions of the transport equations, following an increase in background flux illumination, have been obtained, including the effects of space charge in the near contact region. The modeling results indicate that transient phenomena with time constants on the order of seconds occur due to changes in the electric field and ionized acceptor concentration in the near-contact region.

Acknowledgements

I would like to express my gratitude to Professor Eugene Haller for the generous contribution of time and effort that he has made to my education in the past four years and for his support and supervision of this work both in the laboratory and in many invaluable discussions of the results. Work done in collaboration with Dr. Robert McMurray and Thomas Germer is included in this thesis, and I wish to thank both of them for their contributions and acknowledge their assistance and expertise. The contributions of Professor Robert Westervelt and Stephen Teitsworth of Harvard University to the development of recent photoconductor modeling theory are also gratefully acknowledged, and I thank them for their assistance and hospitality during my visit to Harvard.

Paul Luke was instrumental in beginning the early stages of the infrared detector project, and I would like to thank him for his assistance and insights during the entire course of this work. I am especially grateful to Jeff Beeman for his technical assistance and moral support during the past year. He has made many contributions to our infrared detector program which aided in the completion of this work. William Hansen, Dick Davis, Joe Kahn, and David Nolte have assisted with this work in many areas and I am grateful to them, as well as to many other members of the Lawrence Berkeley Laboratory staff, for the opportunity to benefit from the resources, both in personnel and facilities, of the national laboratory.

It has been my privilege during the course of this project to interact with many people in the infrared detector community and I have benefitted from my involvement in many discussions and projects with

them. I would especially like to express my appreciation to Professor Paul Richards, Mark Hueschen, and Dr. Dan Watson. I am grateful to Professor Eicke Weber and Professor Reinhard Genzel for reading and commenting on this manuscript.

Finally, I wish to express my deepest thanks to family and friends, especially my mother Kathleen Haegel, for their encouragement and friendship along the way. Many people have offered their support, in ways they may never know, and I am deeply grateful to all of them.

I wish to acknowledge the support of a National Science Foundation Graduate Fellowship during three years of my study and also the support of an Atlantic Richfield Corporation Fellowship. This work has been supported by NASA Contract W-14,606, under Interagency Agreement with the Director's Office of Energy Research, Office of Health and Environmental Research, U.S. Dept. of Energy under Contract No. DE-AC03-76SF00098.

TABLE OF CONTENTS

Chapter 1: Introduction and Background

The first conference devoted entirely to the topic of photoconductivity in solids was held in Atlantic City in 1954. The conference proceedings begin with the following statement:

> Photoconductivity is one of the most complex phenomena of solid state physics, involving, as it does, the interaction of light quanta with a solid to produce free charge carriers whose subsequent history reflects all of the fascinating diversions encountered by an itinerant electron or hole in a solid (1).

During the past thirty years, a number of other solid state phenomena may have laid greater claim on the degree of complexity, but the fascinating diversions encountered by itinerant electrons and holes in illuminated solids continues to be an area of great interest.

Photoconductivity, defined as the increase in conductivity of a solid due to the absorption of light, is applied extensively in the characterization of solids, both semiconductors and insulators, and in the detection of radiation in all parts of the electromagnetic spectrum. Over a wide range of infrared wavelengths (5–200 μm), the most sensitive photon detectors are extrinsic Si:X and Ge:X photoconductors, where X is any donor or acceptor impurity with an ionization energy corresponding to the wavelength of interest. These detectors operate at low temperatures ($T<20K$ for Si, $T<4.2K$ for Ge) and can detect small changes in photon streams at very low levels of photon flux.

Current interest in extrinsic photoconductors as far-infrared detectors is driven primarily by new opportunities for space-borne telescopes which allow astronomers to observe infrared sources without the H_2O and CO_2 absorption which limit earth-based facilities. The successful launch and operation of the Infrared Astronomical Satellite

(IRAS) in 1981 greatly improved the sensitivity of infrared observation and led to the detection of about 250,000 infrared sources (2). Plans for future missions include COBE, the Cosmic Background Explorer which will use bolometric devices to measure the cosmic background radiation (3), ISO, the Infrared Space Observatory which is a European satellite covering the 3 to 200 μm wavelength range (4), and SIRTF, the Space Infrared Telescope Facility, which is currently on the drawing board for 1992 (5). The success of these missions is determined in large part by the sensitivity and reproducibility of the extrinsic semiconductor photoconductors and bolometers which are the radiation-detecting elements. The very low background fluxes encountered under space conditions, combined with the interest in measuring increasingly small signals, has led to a renewed interest in the more subtle aspects of photoconductor behavior and characterization under low background.

Efforts to meet the demands from the astronomy community for improved detector performance have been aided by the significant improvements in semiconductor purification and device fabrication in the past twenty years. Improved control of semiconductor doping, the use of implantation for contact formation, and the amazing progress in device integration in Si has led to highly sensitive and sophisticated Si:X detectors which can now be used in integrated two-dimensional arrays (6,7). Ge detectors have also benefitted from improvements in materials development and contacting procedures, although the push toward arrays has been limited by both fundamental problems and the concentration of interest in longer wavelength detection in a smaller and more peaceful, though no less fervent community. In both cases, however, materials development has not been fully exploited and there remain a number of phenomena which are not

fully understood. These include temperature-related changes in behavior, memory effects, large current pulses not related to changes in flux, and the transient responses to changes in flux, bias, or other perturbations. These so-called "anamolous" behaviors become increasingly important as new demands are placed on detector performance.

The goal of photoconductor research for astronomy-related applications is to provide detectors with well characterized behavior which meet performance specifications of sensitivity, speed, wavelength coverage, etc. For the far-IR, this requires the study of lightly doped Ge (10^{14}-10^{15} cm^{-3}) with conditions simulating the space environment. This thesis focuses on research and development of Ge:Be, Ge:Zn, and Ge:Ga detectors. The primary emphasis is on the study of temperature-dependent and transient phenomena in Ge:Be and Ge:Zn photoconductors. These detectors can display transient behaviors characterized by very long time constants (~ 1 sec) which are not fully explained at the present time. In addition, the temperature-dependent behavior of detectors based on "semi-deep" levels offers some interesting possibilities for study and exploitation that are not available in the more common shallow level detectors. An extensive experimental study of these two systems has been undertaken in order to improve the understanding of the fundamental behavior of extrinsic photoconductors.

1.1 Principles of Extrinsic Photoconductivity

The term "extrinsic photoconductor" is used to refer to a material where the photoconductive response of interest is due to the photoionization of impurities, donors or acceptors, which are extrinsic

to the host lattice. This is in contrast to intrinsic photoconductors where one is concerned with the transition of electrons and holes across the band gap. In the wavelength ranges where they overlap, intrinsic photoconductors have several distinct advantages. The light absorbed by a detector in a single pass, excluding the effects of reflection at the front surface, is given by the standard expression

$$I=I_0(1-\exp(-\alpha x)) \qquad (1.1)$$

where $\alpha=\sigma N$ [σ is the photoionization cross-section and N is the concentration of absorbing centers].

Alpha for the band to band transitions is usually several orders of magnitude greater than for the optimally doped extrinsic absorption, due to the larger concentration of absorbing centers. As a result, intrinsic detectors absorb more light in a thinner sample. This is beneficial in a space environment because a smaller volume detector will have less interaction with high energy ionizing radiation such as γrays and protons which interfere with detector performance. In addition, intrinsic detectors are generally used in a photovoltaic or diode mode (n^+-p-p^+ or p^+-n-n^+) while extrinsic photoconductors are most commonly operated as ohmic devices. It can be shown (8) that a detector operated as a photodiode has an ideal signal to noise ratio (S/N) which is a factor of 2 lower than an ohmic photoconductor. This is due to the absence of recombination noise in the photodiode.

Limitations to intrinsic devices arise, however, when one wishes to detect radiation in the far-IR. The smallest III-V bandgap material is InSb, with a cut-off wavelength of ~10 μm. Extensive work is in progress on $Hg_{1-x}Cd_xTe$, a semiconductor with a tunable bandgap as a function of composition, but most recent results report competitive performance

only at short wavelength and high operating temperatures (9). Thus, for wavelengths beyond ~10 μm, it is necessary to use extrinsic photoconductors or bolometric devices. Figure 1 shows the cut-off wavelength and general range of operation of intrinsic detectors and extrinsic Si, Ge, and GaAs.

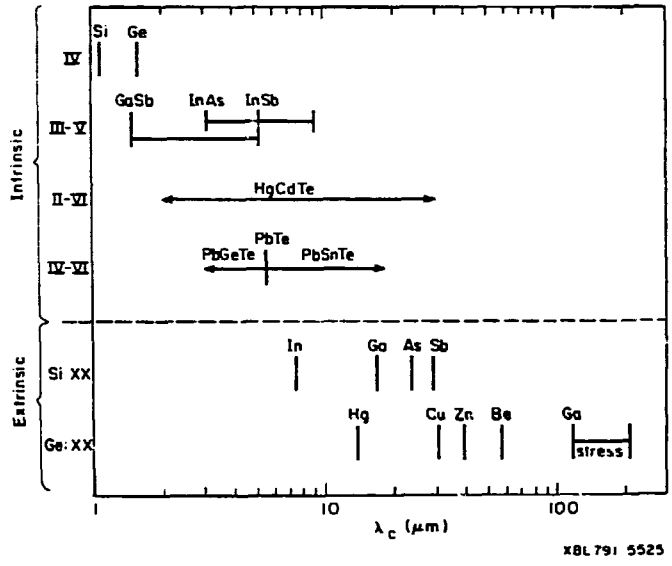

Figure 1
After Richards P L and Greenberg L T, "Infrared Detectors for Low-Background Astronomy: Incoherent and Coherent Devices from One Micrometer to One Millimeter," Infrared and Millimeter Waves, Button K J ed., (New York: Academic Press), 6, 150 (1982).

Extrinsic Ge detectors are used primarily for wavelengths from 30-200 μm. For shorter wavelengths, extrinsic Si detectors have been developed. Due to the advanced state of Si crystal growth and processing, Si:XX detectors (Si:Sb, Si:Ga, Si:In) have replaced the earlier devices based on deep and semi-deep levels in Ge (Ge:Au, Ge:Cu, Ge:Hg). On the long wavelength end, the shallow donor impurities in GaAs seem to offer the potential for detection to 300 μm, although currently the use of GaAs as a far-IR detector is limited to epitaxial layers and bound to excited state transitions (10). Improvements in bulk GaAs will no doubt expand

the use of these detectors.

The basic process of extrinsic photoconductivity is well known and extensively reviewed (11,12). An extrinsically doped piece of semiconductor is cooled to a temperature such that most of the centers are neutral. (To be more precise, virtually all of the centers are neutral. In a Ge:Ga detector at 4.0K, the free hole concentration is approximately 3 cm^{-3} out of $2x10^{14}$ cm^{-3}.) Photons are absorbed via a transition of the hole (electron) from the ground state to the continuum. The resultant change in free hole concentration, $\Delta p=\dot{p}\tau$ where $\dot{p}$ is the flux rate (photons/cm^2sec) and τ is the lifetime of the free carrier (sec), will cause an increase in conductivity. This is observed as a change in either current or voltage depending on the mode of device operation. This process is illustrated in Figure 2.

The expression for the current density though a photoconductor can be written, in its most general form, as

$$j=j_{conduction}+j_{displacement}+j_{diffusion}$$

or

$$j(x,t)=e\mu p(x,t)E(x,t)+\epsilon\frac{\partial E(x,t)}{\partial t}-D_p e\frac{\partial p(x,t)}{\partial t} \qquad (1.2)$$

where e is electron charge, μ is mobility, p is free hole concentration, E is electric field, and D is the diffusivity. A rigorous derivation of the photocurrent equations, based on the assumption of an ideal contact, has been given by Rittner (13).

Commonly, one is concerned with the steady state current flowing through the device under a given flux rate p. In this case, the time derivative goes to zero (i.e., no displacement current). The diffusion

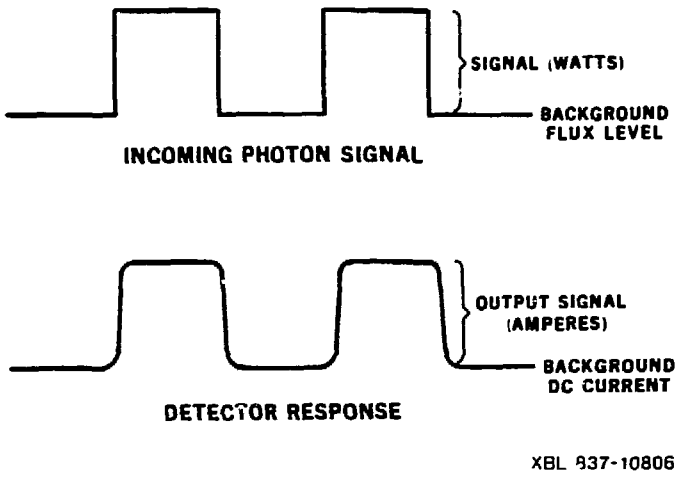

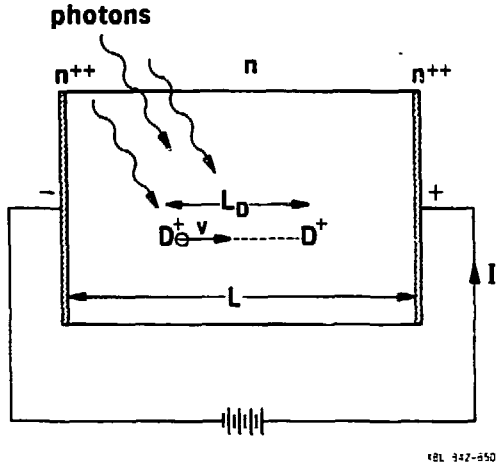

Figure 2
Operation of an Extrinsic Photoconductor

term can generally be neglected in the bulk under the condition of uniform illumination of a homogeneous sample, although this term cannot be neglected in the near-contact region. For bulk steady state

photoconductivity then, Eqn. 1.2 reduces to

$$j(t)=e\mu p(x,t)E(x,t) \qquad (1.3)$$

or, in terms of flux rate and carrier lifetime,

$$j(t)=e\mu\tau\,\bar{p}(x,t)E(x,t). \qquad (1.4)$$

This is the usual starting place for simple analytical studies of current flow in the device. It is obvious that an increment in Δp causes a linear increase in $j(t)$ for cases where the background flux is low enough that μ and τ are flux-independent. However, the behavior of $j(t)$ under non-steady-state conditions (transients) or under conditions where $\tau=\tau(p)$ is not so straight forward and less well understood. These will be the topics, respectively, of Chapters 4 and 3. At that point, it will be necessary to introduce the effects of space charge (Poisson's equation) and the dynamic behavior (continuity of charge carriers). These three equations in combination define all the essential physics to understand the steady state and transient photoconductive behavior.

Phenomenologically, a photoconductor can be thought of as a transducer which converts a photon signal into an electrical signal. Returning to Figure 2, if a single photon is absorbed by a neutral impurity in the detector volume, a free carrier is created. This carrier will exist on the average for a lifetime τ before it is captured by the Coulomb potential of an ionized impurity and recombines. During this time τ, the carrier will move a distance L_d, the drift length, parallel to the applied field E. The photocurrent measured in the external circuit is given by

$$J=pe(L_d/L)=pe(v_d\tau/L) \qquad (1.5)$$

where L is the distance between the electrodes.

If $v_d=\mu E$ (i.e., below saturation velocity), then

$$J=e\mu\dot{p}\tau E \qquad (1.6)$$

which is the same current expression as Eqn. 1.4.

The quantity $\mu\tau E/L$, or more generally, $v_d\tau/L$, is simply the ratio of drift length to intercontact length (or lifetime to transit time), and was defined by Rose (14) as the photoconductive gain G. It is a measure of device sensitivity because the photocurrent for a given photon flux is directly proportional to G. With large electric field or long free carrier lifetime, the photoconductive gain can be larger than one, although values from 0.1 to 1.0 are more common for extrinsic Ge detectors. To understand this, it is useful to think of a photoconductor as the analog of a parallel plate capacitor filled with a dielectric of relative dielectric constant ϵ. The ratio L_D/L is the fraction of unit charge change on the contact plates caused by the motion of free charge within the dielectric. If the drift length of a free carrier is long enough that it does not recombine in a single pass through the device, other carriers injected at the injecting contact continue to influence the mirror charges on the electrodes, causing current flow in the external circuit.

The gain can be a complicated function of chopping frequency and is affected by heating of carriers as well as saturation effects under ac conditions. These behaviors will arise when we consider the transient response of detectors. Primarily, however, the photoconductive gain is a function of the material parameters which determine μ and τ, and it is through the control of these parameters that optimized material is produced for detector use.

1.2 Materials for Photoconductor Applications

A schematic band diagram for an extrinsic, long wavelength p-type photoconductor is shown in Figure 3. The material is intentionally doped with a primary dopant A and contains a residual concentration of compensating donors D. Such a diagram is representative of Ge:Ga or Si:B, cases where the primary dopant is a shallow level and other residual acceptors are not important. This is because they either are of similar ionization energy but orders of magnitude lower in concentration (as for Ge:Ga), or they are both orders of magnitude lower in concentration and have an ionization energy greater than the primary dopant and are therefore neutral and play no role in the photoconductor (as in the case of Al in Si:B).

A more general case, and the case of interest in this work is shown in Figure 4. In this case, the primary dopant is a semi-deep level, but the residual shallow impurities will be shown to affect both the temperature dependence and the transient response of the photoconductor. Figure 4 applies to materials such as Ge:Be and Ge:Zn, considering only the first ionization stage of the double acceptor, as well as to Si:Ga and Si:In. Methods for characterization of multi-level systems to determine the ionization energy and concentration of the various levels will be reviewed in Chapter 2.

In addition to determining the cut-off wavelength for photoconductive response, the dopant impurities determine the free carrier lifetime and mobility and all the low temperature transport behavior. "Optimized" material for photoconductor applications often involves a trade-off between maximum absorption (high $\alpha \propto$ high N) and low dark current (high N leads to hopping or banding conduction), between high photoconductive

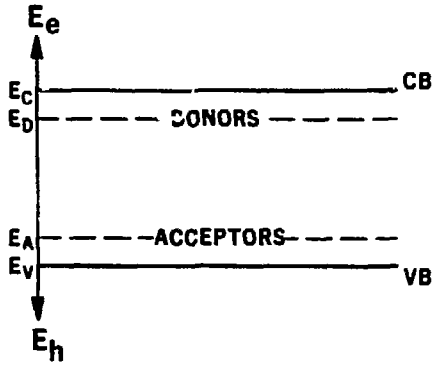

Figure 3
Single level photoconductor band diagram

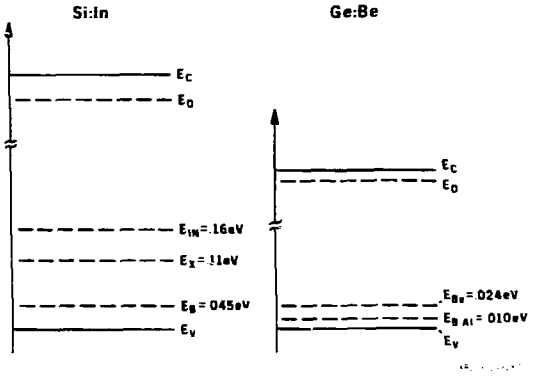

Figure 4
Multi-level photoconductor band diagram

gain and low breakdown field (15), or between high sensitivity and maximum speed. Meeting all these specifications requires control of the doping of the semiconductor with respect to both majority and minority impurities. Improved crystal growth conditions, for both Si and Ge, have contributed to the improved performance and flexibility in detector design.

1.3 Figures of Merit and Detector Performance

No overview of the essentials of far-IR photoconductors for application in astronomy can be complete without a discussion of figures of merit and

detector performance. For low background operation, the two most frequently used figures of merit are responsivity and noise equivalent power (NEP). Responsivity is a measure of signal size and is defined by

$$R = [e/(h\nu)]\, G\eta = [e/(h\nu)](v_d \tau \eta/L) \qquad (1.7)$$

where G is the gain and η is the quantum efficiency for photon absorption. The NEP is a measure of the signal to noise ratio, or alternately the minimum signal required to obtain a signal to noise ratio of unity in a 1 Hz bandwidth. The measured NEP, given by

$$NEP = P_{signal} \times \frac{Noise}{Signal} \qquad (1.8)$$

is compared to the ideal NEP which could be obtained if the noise associated with the signal were only the noise due to the random generation and subsequent independent random recombination of free carriers (16). This is the background limited, or more aptly photon noise limited (pnl) NEP, and is given in the Poisson limit by

$$NEP_{pnl} = 2\sqrt{Ph\nu} \qquad \text{for } \eta = 1 \qquad (1.9)$$

Of course, there are always additional noise sources which may contribute to the total noise signal. These include thermal generation-recombination noise, noise associated with non-ideal contact behavior, and the Johnson noise of feedback resisitors or other amplifier noise. Regardless of which noise source is dominant (usually photon noise or electronic noise), the minimum noise will determine a maximum sensitivity of the detector.

The NEP performance characterisitics of Ge:Be detectors have been evaluated and presented elsewhere (17,18). Figures 5 and 6 summarize the results showing the NEP as a function of bias for several Ge:Be detectors and a comparision of Ge:Be and Ge:Ga results at a wavelength of 42 μm.

One sees that Ge:Be gives better performance than Ge:Ga in this wavelength region and that the performance approaches background limited performance to within a factor of 1.5 assuming a responsive quantum efficiency of one for a detector in an integrating cavity. These detectors will be used on future space missions because of their improved sensitivity. Therefore, a better understanding of their performance under low background conditions is required.

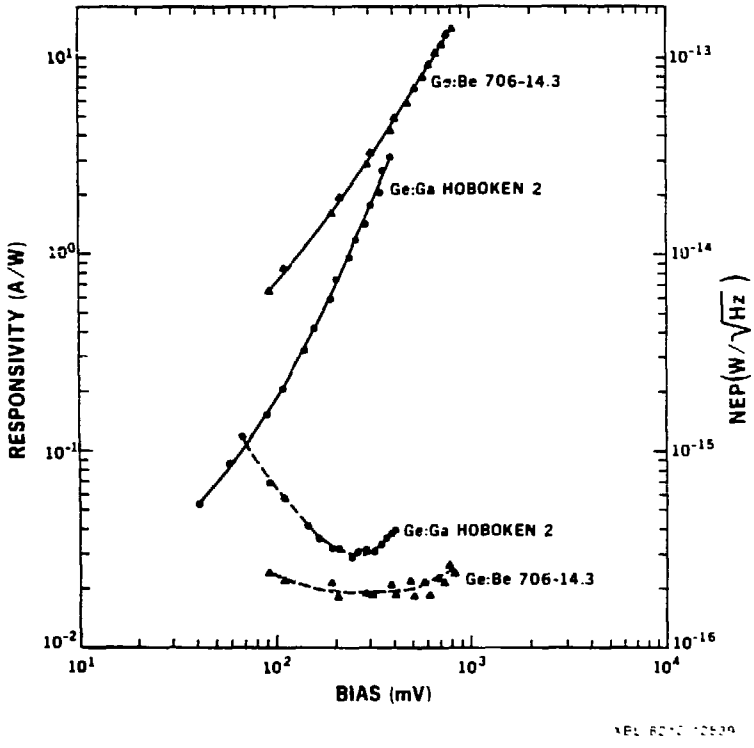

Figure 5
Responsivity and NEP as a function of bias for a Ge:Ga and Ge:Be detector both at λ=42 μm. T(Ge:Ga) = 3.0 K T(Ge:Be) = 3.8 K. $NEP_{pnl} = 1.2 \times 10^{-16}$ W/ Hz Background = 1.5×10^{8} p/s.

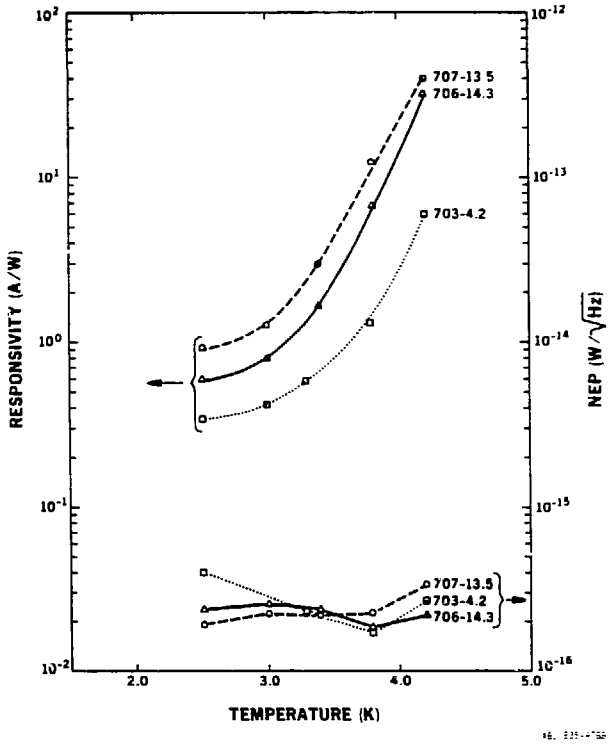

Figure 6

Responsivity and NEP as a function of temperature for three Ge:Be detectors. $NEP_{pnl} = 1.2 \times 10^{-16}$ W/ Hz
Background = 1.5×10^{8} p/s.

Chapter 2: Materials Development and Characterization Techniques

Beryllium occupies a substitutional site and is a double acceptor in Ge with ionization energies of 24.8 and 58 meV (19). Interest in Ge:Be as a detector material is generally limited to the first ionization stage, and the earliest evaluation of Ge:Be photoconductors was published by Shenker, Swiggard, and Moore in 1967 (20). Recent development of Ge:Be has been directed toward producing an optimized detector in the 30-50 μm wavelength range. In addition to the work cited earlier, there were several other efforts in material and detector development (21,22).

Zinc is also a double acceptor occupying a substitutional site in Ge, with ionization energies of 33 and 86.5 meV (19). Ge:Zn detectors were developed in the early 1960's, but were never extensively utilized (24,25). The interest here in Ge:Zn is primarily as an analogous system to Ge:Be, allowing for extension of the experimental survey beyond a single example of a multi-level system. There is less practical application for Ge:Zn detectors in astronomy, since they begin to overlap the wavelength range which can be covered by Si:X detectors and since the Ge:Be detectors have been quite successful.

A schematic spectral response including Ge:Be and Ge:Zn is shown in Figure 7. In studies concerned with the characterization of the far-IR detectors, only the first hole is removed (i.e., first ionization state) and the doubly ionized state is never present. This is accomplished by operating the device at low temperatures and using appropriate filtering so that there is neither thermal nor optical energy to remove a second hole. The compensating donor concentration is always low enough ($N_D << N_{Be}$) so that no doubly ionized centers are formed due to compensation.

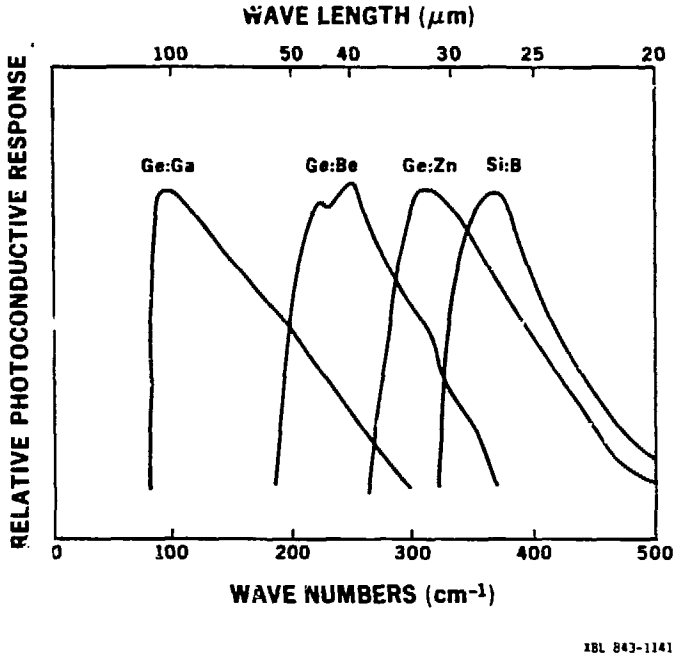

Figure 7
Schematic spectral response for Ge:Be and Ge:Zn

2.1 Single Crystal Growth

2.1.1 Ge:Be Single Crystal Growth

In addition to the wavelength associated with its first ionization energy (Be is the shallowest of the deep multivalent acceptors in Ge), the high solubility of Be in the Ge lattice makes it especially suitable as a dopant for a photoconductor. Unlike the other deep double acceptors (Zn, Cd, Mn, Co, Ni, Hg), Be is as soluble in the lattice as the more commonly used Group III and Group V dopants. Shenker et.al. (20) reported a maximum solubility in excess of 10^{19} cm^{-3}, and a maximum solubility of ~ $4x10^{20}$ cm^{-3} at the crystallization temperature has been calculated (26). The limiting factor, therefore, in the doping of Ge:Be for photoconductor applications is the onset of significant hopping conduction and not the solubility. This is beneficial since one generally desires to have as large a concentration of dopant as possible

in order to maximize the probability of photon absorption in single pass applications.

Because Be readily oxidizes, problems are encountered in crystal growth which are not present, for example, when doping with Ga. The oxygen content of the melt environment (crucible and surrounding atmosphere) is the critical factor in determining whether Be will precipitate as stable and neutral BeO or remain as an isolated dopant which is electrically active.The standard conditions for high-purity Ge Czochralski crystal growth (27) require a silica crucible and a Pd-diffused H_2 atmosphere. Thermodynamics calculations, based on the free energy of formation and the mass action law, can be done to give an indication of the stability of an oxide under such conditions.

In the earlier stages of this work, these calculations were performed following the method used by Darken (28). Two conclusions were reached:

1) Stable BeO would be expected to form in equilibrium under a H_2 atmosphere when the ratio of partial pressures of water to hydrogen exceeds 5.5×10^{-7} for growth at 1200 K with a Be concentration of 5×10^{15} cm^{-3}. Since the dryness of the hydrogen generally attained is only a partial pressure ratio of 10^{-5}, the formation of stable BeO is very likely under a H_2 atmosphere.

2) Within the limits imposed by the kinetics of diffusion and convection, Be will reduce a SiO_2 crucible. The Be in the melt could be depleted by the following reaction:

$$2Be_{(m)} + SiO_2 \rightarrow 2BeO + Si \qquad (2.1)$$

The form of the calculations is presented in Appendix 1 and subsequent experience has verified their predictions. Generally the problem was solved by growing the crystals in a less oxygen-rich

environment by removing the silica crucible and growing directly from the carbon susceptor under vacuum (10^{-6} to 10^{-7} torr). Significant loss of Be was not observed under these conditions. In cases where it was necessary to grow under a H_2 atmosphere (see Chapter 3.3), loss of Be during crystal growth was observed. Figure 8 shows the concentration profiles along the length of the crystal for a number of representative crystals and illustrates this effect.

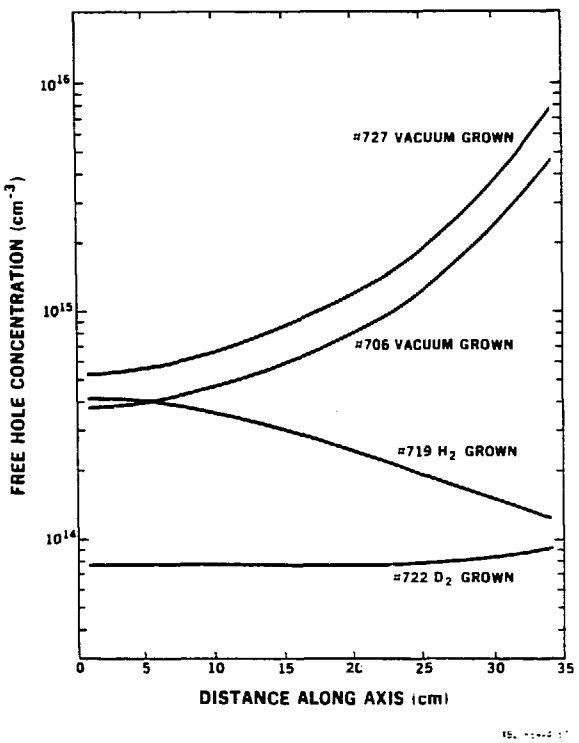

Figure 8
Concentration profiles along the length of Ge:Be crystals for growth under vacuum and H_2

The Be concentration required for optimum photoconductor material is approximately 10^{15} cm^{-3}, less than one part per billion. At such small concentrations, direct doping with pure Be is very inaccurate. Doping of the melt with Be was achieved by adding a small piece of

heavily doped master alloy to the high purity zone refined charge. The master alloy was prepared by alloying pure Be and Ge. The resultant average concentration of electrically active Be in the master alloy was $\sim 3 \times 10^{18}$ cm^{-3} as measured by room temperature Hall effect. Use of a master alloy provides a more controlled method of doping than direct addition of Be to the melt. The weight of the master alloy required is generally about one gram. This can be measured much more accurately than the micrograms of Be metal which direct doping would require. A Hall effect measurement can be used to determine the Be concentration in the master alloy.

The calculations for determining the weight of the master alloy, given a desired concentration at the seed end of the crystal, are straight forward. The following expression gives the concentration along the length of a crystal for segregation during normal freezing (i.e., solidification from a melt):

$$C(x) = C_o k \, (1-x)^{k-1} \qquad (2.2)$$

where k is the effective segregation coefficient and x is the fraction of the melt which is frozen. The literature value for the equilibrium segregation coefficent for Be in Ge is given as 0.08 (26). Under our growth conditions, the effective segregation coefficient has been determined from the crystal growth profiles to be approximately 0.25.

In addition to the primary dopant, residual impurites such as boron, aluminum, phosphorus, arsenic, etc. are always present, both in the poly-crystalline charge and as contaminants in the crystal growth environment. In Ge:Be or Ge:Zn, the n-type dopants (P,Sb,As) determine the free carrier lifetime and their concentration is extremely important for device performance. The lowest net concentration of residual

electrically active impurities (primarily P) that can be obtained under high purity growth conditions is 10^9-10^{10} cm^{-3}. When a master alloy is used, or when the H_2 atmosphere or SiO_2 crucible is removed, this value rises to 10^{11}-10^{12} cm^{-3}.

The residual p-type impurities (primarily B and Al) will also play a significant role in both the electrical and optical characteristics of the detector. Boron and aluminum are present in the zone-refined charge and can also be introduced by the crucible in contact with the melt. When crystals are grown directly from the carbon susceptor, an increase in the electrically active concentrations of B and Al is observed. This is believed to be due to the effect of B contamination in the crucible and also to the lack of O_2 which would otherwise lead to the precipitation of aluminum oxides. It is these residual impurities, of the same type as the primary dopant, but several orders of magnitude lower in concentration, that cause all photoconductors based on semi-deep or deep levels to be classified as multilevel systems.

Counterdoping is a term that refers to the intentional addition of minority dopants in order to compensate shallow levels. The reasons for and effects of this will be presented in Chapters 3 and 4. The required counter-doping is calculated and carried out in the same manner as the primary doping. In this work, master alloys of Ge:P and Ge:Sb were used.

2.1.2 Ge:Zn Single Crystal Growth

The problems presented by Ge:Zn crystal growth are different than those for Ge:Be, and perhaps more formidable in practice. Although Zn does not oxidize as readily as Be, it does have a very high vapor pressue (1.27×10^3 torr at 960°C) and so tends to evaporate from the melt during

crystal growth. This has two effects. First, it depletes the melt of electrically active Zn and causes a change in the segregation profile similar to that for depletion of the melt due to oxidation. Secondly, it leads to serious contamination of the high purity Ge crystal growth facility. Growth of material doped with high vapor pressure dopants (Zn, Hg, Cd) is normally done by vapor doping in a sealed capsule (11). Alternately, a zone leveling technique is used in which the dopant can be added at several points during crystal growth. Since neither of these options was applicable or desirable for use in our laboratory, a limited number of crystals were grown using the Czochalski technique.

The Ge:Be and Ge:Zn crystals grown throughout the duration of this work are summarized in Table 1. All the materials for photoconductive devices were taken from these crystals. This collection no doubt represents the largest reserve of beryllium doped Ge existing in the world today.

2.2 Variable Temperature Hall Effect

In addition to photoconductivity measurements, three electrical techniques have been used to characterize the detector material: variable temperature Hall effect, photo-Hall effect, and deep level transient spectroscopy. The latter technique has been used only when questions of possible deep level contamination arose and will not be extensively discussed. By far the most important information concerning the electrical and optical behavior of a device based on a multilevel semiconductor is obtained from variable temperature Hall effect measurements.

TABLE 1

Ge:Be and Ge:Zn Single Crystal Material

Crystal	Growth Condition	Master Alloy	Residual doping
Ge:Be			
703	Carbon susceptor, vacuum	Ge:Be	Head: $N_A > N_D$ Tail: $N_A > N_D$
706	Carbon susceptor, vacuum	Ge:Be	Head: $N_A > N_D$ Tail: $N_A \simeq N_D$
707	Carbon susceptor, vacuum	Ge:Be	Head: $N_A > N_D$ Tail: $N_A > N_D$
710	Carbon susceptor, vacuum	Ge:Be Ge:P	Head: $N_D > N_A$ Tail: $N_D > N_A$
719	Carbon susceptor, H_2	Ge:Be	Head: $N_A > N_D$* Tail: $N_A > N_D$*
722	Carbon susceptor, D_2	Ge:Be	Head: $N_A > N_D$*
727	Carbon susceptor, vacuum	Ge:Be Ge:Sb	Head: $N_A > N_D$ Tail: $N_A > N_D$
728	Carbon susceptor, H_2	Ge:Be Ge:P	Head: $N_A > N_D$* Tail: $N_A > N_D$*
Ge:Zn			
714	SiO_2 crucible H_2	Ge:Zn	Head: $N_A > N_D$* Tail: $N_A > N_D$*
715	Carbon susceptor N_2	Ge:Zn	Head: $N_A > N_D$ Tail: $N_D > N_A$

*As grown condition including H-related complexes.

Hall effect measurements in combination with resistivity measurement yield independent values for the free carrier concentration and mobility. The theory for the freeze-out of extrinsic semiconductors under thermal equilibrium is well established and reviewed (29). These equations are summarized and a brief description of the apparatus is given in Appendix 2. Variable temperature Hall effect data are necessary for the characterization of multilevel systems because any room temperature measurement is dominated by the primary dopant. There are no neutral Be or Zn centers at room temperature, and these impurities are present in concentrations of 10^{14}-10^{15} cm^{-3}. Clearly this concentration of free holes makes it impossible to learn anything about residual impurities at a level of 10^{11} cm^{-3}. Only by making the measurement of free carrier concentration over a wide temperature range can the contribution of the shallow levels be observed. This is illustrated schematically in Figure 9 for Ge:Be. In case B, $N_D > N_{A(shallow)}$, and the shallow acceptors are fully compensated at all temperatures. They do not contribute any free holes. If $N_{A(shallow)} > N_D$, then $N_A - N_D$ acceptors remain which will be neutral at T=0 K. Their effect on the free hole concentration at low temperatures can be seen in case A.

In practice, the data obtained from variable temperature Hall effect in Ge:Be and Ge:Zn does not appear like the schematic pictures. The ionization energies of the first ionization of Be and Zn (24.5 and 33 meV) and the ionization energy of the shallow acceptors (~11 meV) are close enough that long plateau regions are not observed. Estimates of absolute concentrations are made from the points where the slope changes. Figure 10 shows two actual examples of materials which illustrate the schematic cases of Figure 9.

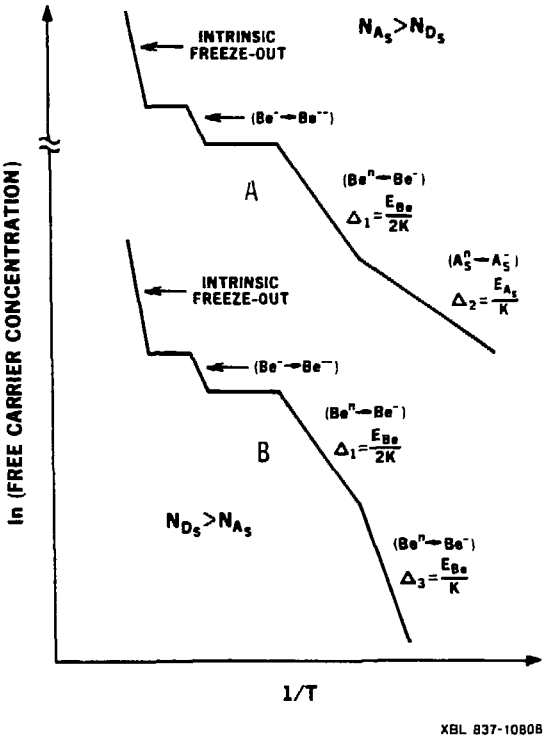

Figure 9
Freeze-out curves for under- and over-compensation of shallow levels in Ge:Be

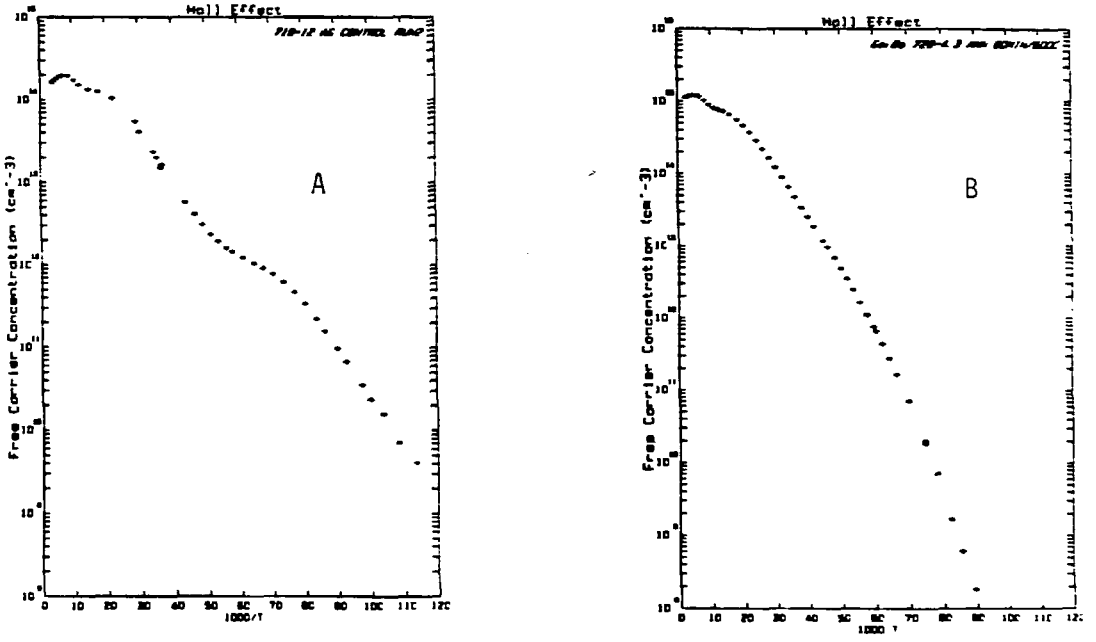

Figure 10
Freeze-out curves for A) $N_{A_S}>N_D$ and B) $N_{A_S}<N_D$

One effect of the residual shallow levels on the performance of a photoconductor is immediately evident from consideration of Figure 10. Two materials, with the same concentration of Be, can have free carrier concentrations differing by many orders of magnitude at T = 4.0 K. Resistivity data (Figure 11) from these two samples illustrate the point more clearly. In the absence of any photon flux, or with a very low photon flux, sample A would have significantly less "dark current", or background current, than sample B. This means less noise associated with thermal generation and recombination and a potentially more sensitive detector depending on observing requirements and background flux.

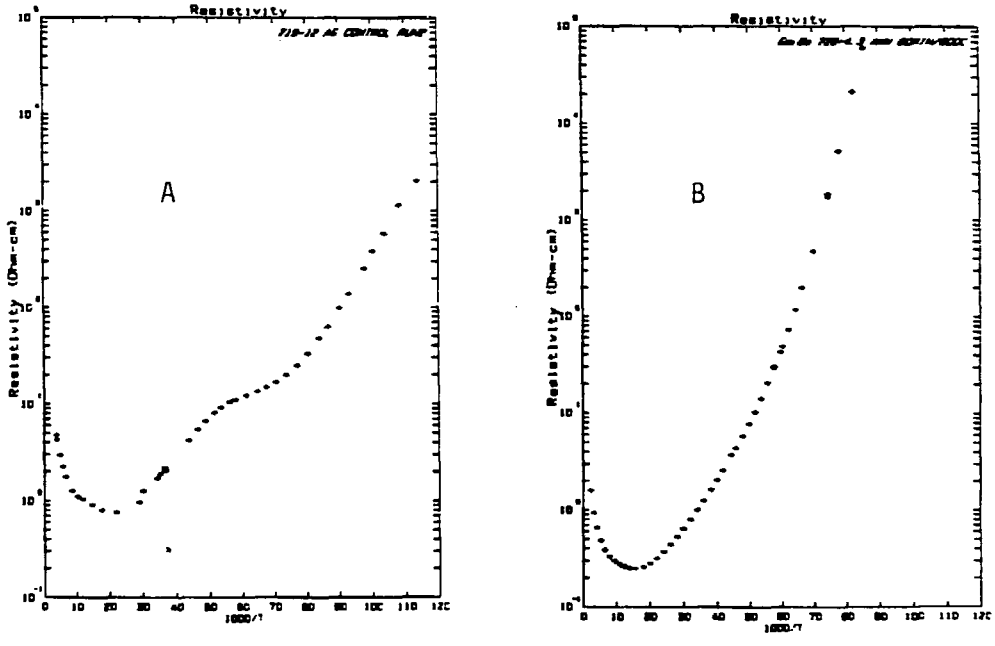

Figure 11
Resistivity versus inverse temperature for samples of Figure 10

Mobility data at low temperatures are also necessary to fully characterize the photoconductor. Photoconductivity measurements lead to a value for the responsivity, or photoconductive gain, which is a product of mobility and lifetime. An independent measurement of $\mu(T)$ is required in order to determine the free carrier lifetime. The various mechanisms for carrier scattering and their temperature dependence will be discussed in Chapter 3.

Variable temperature Hall effect measurements were performed on all the crystals listed in Table 1. Quantitative results will be presented as required, but the qualitative results are included in Table 1. One sees that $N_{A(shallow)}>N_D$ was the more common result from our crystal growth conditions. Complete compensation of shallow levels was generally only achieved with counterdoping.

2.3 Photo-Hall Effect

Photo-Hall effect simply measures the free carrier concentration as a function of temperature in the presence of a photon flux $\dot{p}$. There are two important pieces of information which can be obtained from photo-Hall effect which cannot be obtained from the freeze-out measurements in thermal equilibrium in the dark. In many cases which are of interest in this work, the residual shallow acceptor and donor concentration are quite close ($N_A \approx N_D$) and only an indication of the net concentration $[N_A - N_D]$ is obtained from the Hall effect result. Also, data from Hall effect in the dark does not provide any information about free carrier lifetime.

In the presence of a photon flux, however, the free hole concentration at sufficiently low temperature wil be dominated by optical

generation. If the hole concentration p(T) is expressed as

$$p(T) = p_{thermal} + p_{optical} \quad (2.3)$$

$$= N_v \exp(E/kT) + \dot{p}\tau \quad (2.4)$$

and, if the thermal term is negligible, then

$$p(T) = \dot{p}\tau = \dot{p}/(N_D \sigma \langle v \rangle) \quad (2.5)$$

where N_D is the compensating donor concentration, σ is the recombination cross section, and $\langle v \rangle$ is the mean thermal velocity of the free carriers.

For a known flux, then, the photo-Hall data provides a measurement of the free carrier lifetime. In addition, if $p \ll N_D$ and if the recombination coefficient is known, then the absolute donor concentration can be determined. In combination with standard Hall effect data, all the doping parameters can, in theory, be determined.

The photo-Hall effect has been used primarily in this work to determine $\tau(T)$ over a wider temperature range than can be studied with the photoconductive devices. The photo-Hall effect work presented in this thesis was performed by Thomas A. Germer as part of a senior thesis in the Physics Department, UC Berkeley.

2.4 Photoconductor Fabrication

Selection of photoconductor material from points along the axis of the ~1 kg Czochralski-grown crystals was based on room temperature resistivity measurements to determine Be or Zn concentration and Hall effect data on the residual shallow levels. Optimum Be concentration for photoconductors has previously been determined to be approximately 5×10^{14}-1×10^{15} cm^{-3} (17). Extensive performance characterization of Zn detectors has not been done, but a value of approximately 10^{15} cm^{-3}

or slightly higher would be expected to be an optimum value. Slices of ~1 mm were cut perpendicular to the crystal growth axis (<113> for most cases considered here). The thickness of the slice was determined by the desired inter-electrode distance and varied over a range from 0.2 to 3.0 mm. One mm was the standard value for all results unless otherwise stated.

The slices were lapped with #600 SiC grit to remove saw damage. The wafer surfaces were polish etched in a 4:1 mixture of HNO_3:HF, rinsed with electronic grade methanol, and dried with boil-off N_2. Immediately prior to implantation, the Ge slice was immersed in 1% HF to remove surface oxide. Boron implanted layers ($1x10^{14}$ cm^{-2}, 25keV and $2x10^{14}$ cm^{-2}, 50 keV) were used to provide degenerately doped p+ contacts at low temperatures (30). (A discussion of the theory of implanted contacts is presented in Chapter 5.1) Layers of Ti or Pd (500 Å) and Au (8000 Å) were deposited by Ar sputtering to protect the implanted layer and provide areas for electrical contacts as well as mechanical mounting. After metallization, the finished slices were heated to 300°C for approximately one hour under Ar gas to anneal damage from the implantation and relieve stress in the metal layers.

Final devices of desired geometry were cut from the finished wafer. A common detector size was 1x1x3 mm^3 with 1 mm between the contacts. The bare detector surfaces were polish etched as previously described. The Au layer is not attacked by the etchant. Detectors were either soldered with pure In or glued using a silver-loaded epoxy to a 1 mm diameter carbon steel shaft and then mounted inside a brass integrating cavity with a 1 mm aperture (Figure 12). Integrating cavities are often used in the testing of Ge detectors because of the small value of the

absorption coefficient which leads to a small quantum efficiency for single pass configurations.

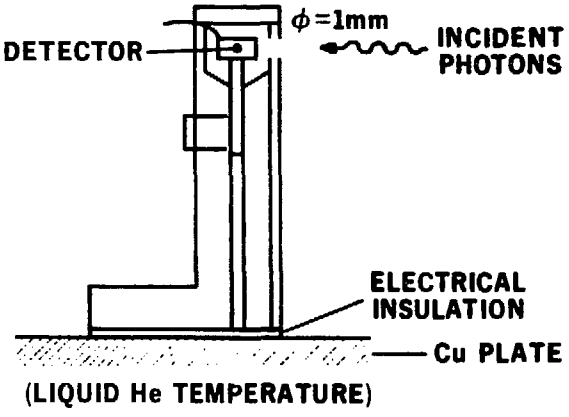

Figure 12
Detector configuration and mounting

2.5 Photoconductivity Measurements

In order to evaluate photoconductive behavior under the low background conditions encountered in space applications it is necessary to have a specially designed cryostat in which all stray radiation is eliminated from the detector environment. The dewar used for photoconductor testing is shown in Figures 13 and 14. It was obtained from Infrared Laboratories, Tucson, AZ (Model HD3). A liquid helium space with a volume of approximately one liter is shielded with a liquid nitrogen temperature jacket. A common vacuum space provides thermal insulation as well as an evacuated space for the detector. The working area is a thick copper plate in contact with the liquid helium bath. The detector in its cavity and all its surroundings are heat sunk to this

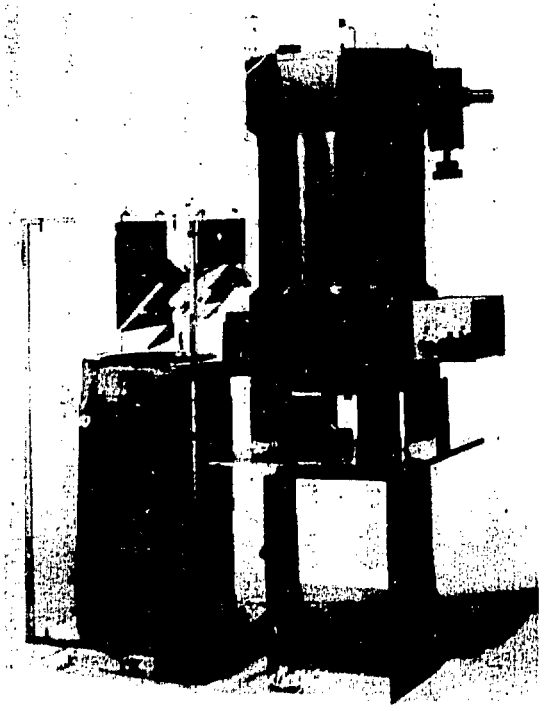

Figure 13
External view of testing dewar and chopper

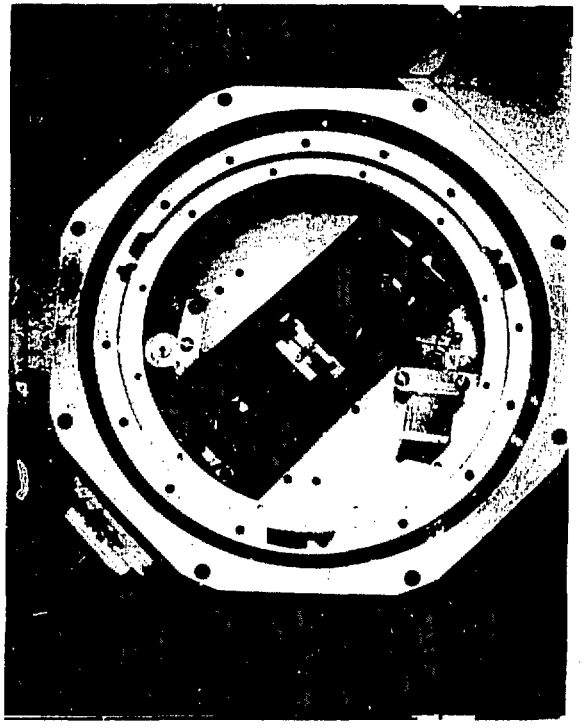

Figure 14
Internal view showing detector, filters and preamplifier

plate with screws and pure In foil.

The photon signal incident upon the detector is produced externally and cold-filtered within the dewar. An external Au-plated metal chopper is used to switch the IR source between variable temperature blackbodies. Most commonly the signal was produced by chopping between a 77 K blackbody (immersed in LN) and the 300 K radiation from the back wall of the chopper box. An Electro-Optical blackbody source (Model 311) with a temperature range of 20-1000°C was also used as a radiation source. Inside the dewar, a rotating wheel with a mechanical connection to the outside allows an internal aperture (ϕ=1 mm) to be opened and closed.

The low background condition for detector testing is achieved with a combination of reduced filter transmission and the geometrical factor imposed by the size of the apertures and the distance between them. Although an exact value for the photon flux was generally not required for the evaluation of the transient and temperature dependent behavior, such calibration is critical in determining absolute values for detector performance such as responsivity and NEP. At these wavelengths it is also necessary to perform a diffraction analysis of the relevant geometry (18

The narrow band filter trains consist of Fabry-Perot mesh filters and Reststrahlen salt filters (31). These filters were fabricated and characterized by D. M. Watson in Professor Charles Townes' group in the Physics Department, UC Berkeley. Table 2 contains descriptions and measured tranmissions for the filters used for testing at 36 and 42 μm. The filters are independently mounted along the optical axis on sliding baffles and are heat sunk directly to the copper plate by two screws and pure In foil.

TABLE 2

Filter Characteristics

λ_{peak} (μm)	Components	Trans (%)	BW (μm)	Q
42.8	42 μm Fabry Perot 0.7 mm LiF 0.5 mm KBr 2 monolayers 5-10 μm diamond dust	13	0.79	85 ± 4
36.6	36 μm Fabry Perot 0.7 mm LiF 0.5 mm KBr 2 monolayers 5-10 μm diamond dust	7.8	1.09	52 ± 2

The detector is located inside its integrating cavity at the far end of a Cu box. Special care was taken to make the box light tight. A double cover with a meandering pump-out groove was used, and all surfaces within the box are covered with 3M flat black paint so that, with the shutter aperture closed, the detector should see no other radiation than the 4K blackbody radiation of its surroundings. The glass feedthrough for the detector leads is opaque to far-IR radiation.

The photoconductor signal is amplified by a standard transimpedance amplifier (32) shown in Figure 15. The input stage consists of two matched junction FETs (J230 selected by Infrared Laboratories). The JFETs are located inside a light-tight Cu housing with opaque feedthroughs. They are mounted off the liquid helium temperature plate on a thin wall fiberglass tube. A 1 kΩ resistor is glued with epoxy to the JFETs. A constant voltage applied across the resistor together with

the power dissipated by the JFETs keeps the operating temperature at approximately 77 K.

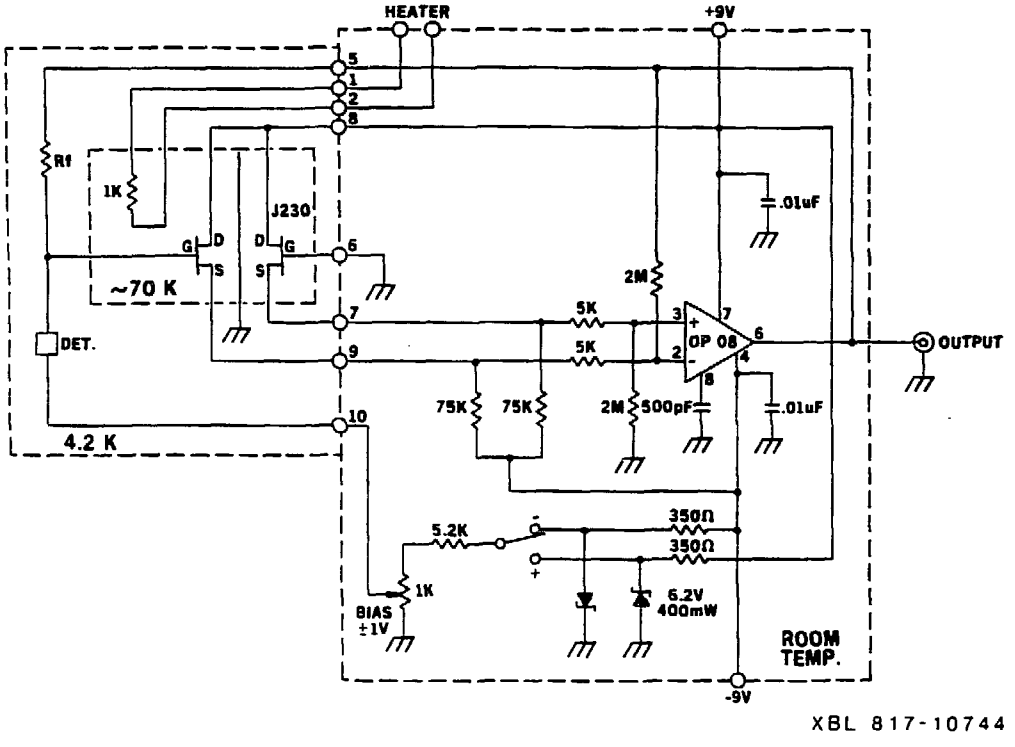

Figure 15
Transimpedance amplifier (TIA) schematic

The feedback resistor connecting the ouput to the gate of the FET is generally an Eltec Model 102 with a room temperature resistance of $10^{10}\Omega$. For lower impedance detectors or for elevated temperature operation, $10^{9}\Omega$ resistors are sometimes used to increase the range of measurable currents. The voltage drop across the feedback resistor (i.e., the output voltage) is divided by the feedback resistance to obtain the value of the current flowing through the detector under fixed bias voltage.

Chapter 3 Temperature Dependence of the Responsivity in Multi-level Systems

3.1 Theoretical Background

The responsivity of a photoconductor, defined in Eqn. 1.6, is temperature-dependent because both the free carrier lifetime and the mobility may be functions of temperature. If one considers first a simple system, such as Ge:Ga, in which there is one acceptor level and compensating donors, then it is easy to derive an expression for the free carrier lifetime. The lifetime of the free hole will be determined by the number of ionized acceptors (N_i^-) with which it can recombine and the capture cross section associated with each center. Ionized acceptors are produced either through photo- or thermal ionization of neutral acceptors or through compensation by donors (i.e., $N_i^-=p+N_D$). The free carrier lifetime τ is given by

$$\tau = \frac{1}{\sigma \langle v \rangle N_i^-} \tag{3.1}$$

If one considers only cases of very low photon backgrounds, and low temperatures such that thermal generation is negligible, then $p \ll N_d$ and

$$\tau = (\sigma \langle v \rangle N_D)^{-1} \tag{3.2}$$

The lifetime is therefore inversely proportional to the compensating donor concentration in p-type material, and so the responsivity, as well as the electrical response time of the device, are determined by the degree of counterdoping.

The temperature dependence of the lifetime arises then from changes in the capture cross section and mean thermal velocity. The latter is given by

$$\langle v \rangle = \left(\frac{8kT}{\pi m^*} \right)^{1/2} \tag{3.3}$$

assuming an average velocity for a Maxwell-Boltzmann distribution. This

assumption is often used because the free carrier energy distribution is unknown. The earliest theory for the temperature dependence of the capture cross section was developed by Lax in 1960 (33) and remains the generally accepted model today, although some modifications have been suggested (34). Lax proposed a model in which the free carrier is captured in a "cascade" process in which it gives up its energy in a series of phonon producing transitions through the excited states of the ionized center which has a screened 1/r Coulomb potential. This analysis led to a temperature dependence of T^{-4} for σ. Abakumov in 1978 suggested that Lax's calculations of the sticking coefficent, a measure of the probability of recombination at each excited state, for the various excited states were incorrect and that the temperature coefficient was actually T^{-3} at higher temperatures and T^{-1} at low temperatures. A collection of literature values complied by Abakumov is given in Figure 16 for capture by various impurity centers in Ge.

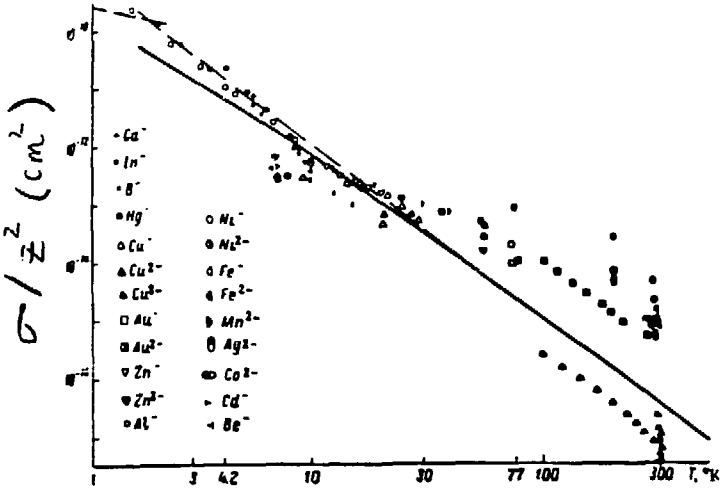

Figure 16
Capture cross section for free holes by ionized centers in Ge (Ref. 34)

The mobility of free holes in p-type Ge has been modeled extensively. Table 3 summarizes the contributions of phonon, charged impurity, and neutral impurity scattering and lists appropriate references. At the temperatures at which Ge photoconductors are usually operated (T<10 K), one sees that the impurity related scattering is dominant. The value of the mobility at any given temperature, as well as the temperature dependence in any temperature range will be determined by the concentration of both neutral and charged impurity centers and their relative contributions to free carrier scattering.

TABLE 3

Scattering Mechanisms in P-type Ge

Mechanism	$(cm^2/(V\ sec))$	Reference
Acoustic phonon	$\mu_l = 3.4\times10^{7}T^{-1.5}$	1,2,3
Ionized impurity	$\mu_i = \frac{1.7\times10^{18}T^{1.5}}{N_D \ln(1 + 8\times10^{8}T^{2}N_D^{-2/3})}$	3,4
Neutral impurity	$\mu_n = 1.1\times10^{20}/(N_A-N_D)$ *	3,5,6

1. Norton P and Levinstein H, Phys. Rev. 80, 72 (1950).
2. Brown D M and Bray R, Phys. Rev. 127, 1593 (1962).
3. NASA CR-166,605 "Conceptual Design of a Hybrid Ge:Ga Detector Array, Aerojet Electro Systems Co., Azusa, CA
4. Conwell E and Weisskopf V F, Phys. Rev. 77, 388 (1950).
5. Erginsoy C, Phys. Rev. 79, 1013 (1950).
6. Blakemore, J S Phys. Rev. B 22, 743 (1980).

* Value for Ge:Ga - depends on specific dopant

Combining the effects for both μ and τ, one obtains the following temperature dependence of responsivity for the operating temperature range of Ge:Ga photoconductors:

$N_A >> N_D$ (neutral impurity scattering) $R \sim T^{2.0}$

$N_A > N_D$ (charged impurity scattering) $R \sim T^{3.5}$

In a multi-level system, however, the temperature dependence of the responsivity is more complicated and can be much more strongly temperature-dependent. The first evidence of this was observed in Si:In detectors developed for the 3-5 μm atmospheric window. Models which explain this behavior have recently been proposed (35,36) and the agreement with experimental results for Si:In has been good. These models should also be applicable to the temperature-dependent behavior for Ge:Be and Ge:Zn, with appropriately scaled temperatures and electric field effects to reflect the smaller binding energies of shallow levels in Ge.

The model proposed by Alexander et.al. (35) is based on the calculation of the generation-recombination equilibrium in a space charge neutral detector under a constant background flux Q. One obtains an expression for the derivative of the hole concentration with respect to flux (dp/dQ) as a function of temperature. The results of the model are summarized in Table 4. One sees that for very close compensation of the shallow acceptors ($N_A \approx N_D$), large values of responsivity are predicted since the value of dp/dQ increases exponentially with temperature.

Phenomenologically, the model predicts that there will be a large step-like increase in free carrier lifetime as a function of temperature in detectors where the shallow levels are closely compensated. The increase in lifetime begins to occur approximately at the point when

TABLE 4

Temperature Dependence of Responsivity for Multi-level Materials*

	$N_A > N_D$	$N_A = N_D$	$N_A < N_D$
T_1	$R \sim \frac{N^O \sigma}{N_D g C}$	$R \sim \frac{N^O \sigma}{N_D g C}$	$R \sim \frac{N^O \sigma}{N_D g C}$
T_2	$R \sim \frac{N^O \sigma}{N_D g C}\left(\frac{N_B}{(N_B - N_D)}\right)$	$R \sim \sqrt{\frac{N^O \sigma}{N_B g C Q}}\, e^{-(E_B/2kT)}$	$R \sim \frac{N^O \sigma}{(N_D - N_B) g C}$
T_3	$R \sim \sqrt{\frac{N^O N_v}{g}}\, e^{(E^O/kT)}$	$R \sim \sqrt{\frac{N^O N_v}{g}}\, e^{(E^O/kT)}$	$R \sim \sqrt{\frac{N^O N_v}{g}}\, e^{(E^O/kT)}$

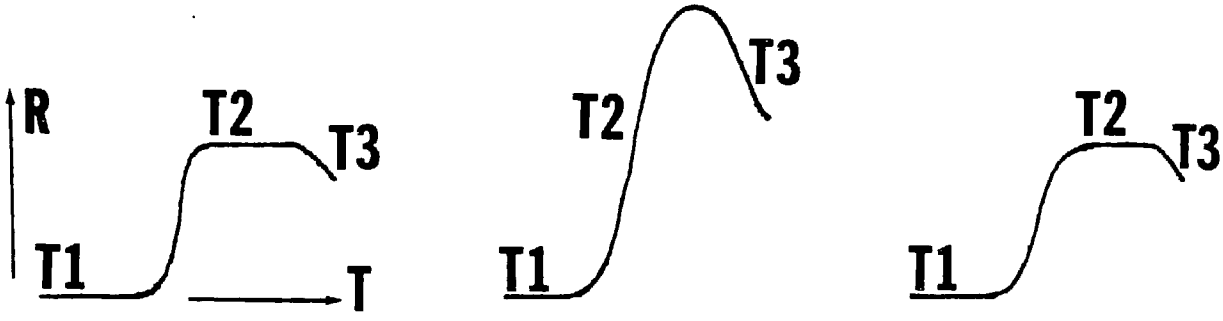

E^O - ionization energy of primary dopant (eV)
N_A - shallow acceptor concentration (cm^{-3})
N_D - donor concentration (cm^{-3})
R - responsivity
N^O - primary dopant concentration (cm^{-3})
σ - optical cross section (cm^2)
g - degeneracy factor
C - recombination coefficient (cm^3/sec)
Q - photon flux ($cm^{-2}s^{-1}$)
N_B - shallow acceptor conc. (assuming B dominant)
E_B - shallow acceptor ionization energy (eV)
k - Boltzmann's constant (eV/K)
T - temperature (K)

* Assuming an acceptor majority dopant. Subscripts can be transcribed symmetrically for n-type material. N_A refers only to shallow residual levels and does not include primary dopant

$$T_c = \frac{E_A}{k \ln \left(\frac{N_v}{gp} \right)} \qquad (3.4)$$

i.e., when the rate of thermal generation from the shallow levels becomes large with respect to photogeneration. This process is illustrated in Figure 17. The case at left represents the photoconductor at temperatures $T<T_{critical}$ where photogeneration of holes is the dominant process from both levels. In this case, the shallow acceptors are neutral; they are initially ionized due to compenstion but then capture free holes. The probability of ionization due to photoionization is small because of the much larger concentration of the semideep level. This equilibrium state in the presence of a photon flux is in direct contrast then to the equilibrium state in the dark. The semi-deep level will be partially ionized rather than the shallow levels.

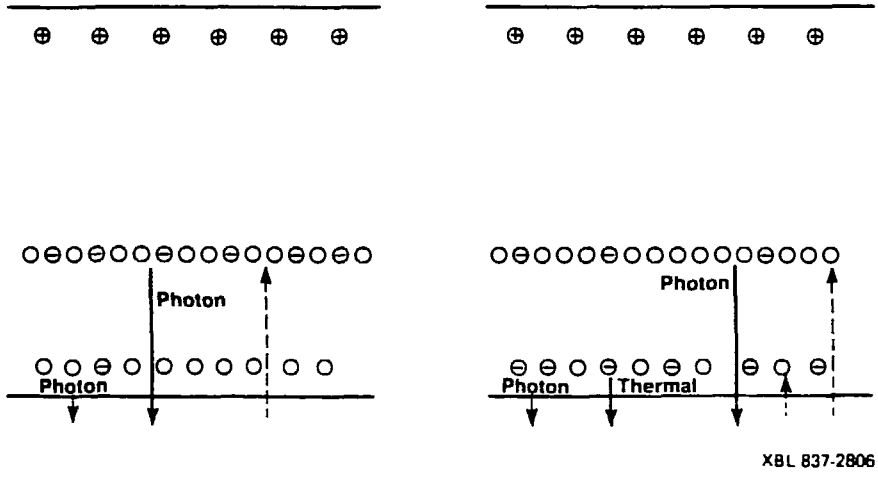

Figure 17

As the temperature is increased, thermal generation from the shallow levels becomes important and the number of ionized shallow levels increases. In the exactly compensated case, it is possible for the shallow acceptors to become fully ionized due to thermal generation. Free holes have a small probability of recombining into the ground state, leading to very long carrier lifetimes and high responsivities. One must keep in mind during this analysis that we assume that the number of ionized sites due to photoionization is small compared to the number due to compensation. This is always true in the operation of low background detectors.

3.2 Modeling of Ge:Be Experimental Results

Data showing this strongly temperature dependent behavior in Ge:Be were first published in 1982 (17). Figure 18 shows a log-log plot of responsivity versus temperature for a number of Ge:Be detectors, showing in several cases the strong deviation from the power law dependence which would be expected from considering only the temperature dependence of the capture cross section. In one case, the temperature range has been extended beyond 4.2 K to show the R(T) behavior after the step. Sample 710-14.3 was taken from a crystal which was intentionally counterdoped so that the shallow acceptors were overcompensated. In this case, no strong temperature dependence is observed.

The model proposed by Alexander et.al. would appear to apply directly to the case of Ge:Be and to explain qualitatively all the observations. However, there are several features requiring further discussion. First, the modeling done by Alexander et.al. neglects the temperature dependence of the recombination coefficients, and therefore comparison of experiment

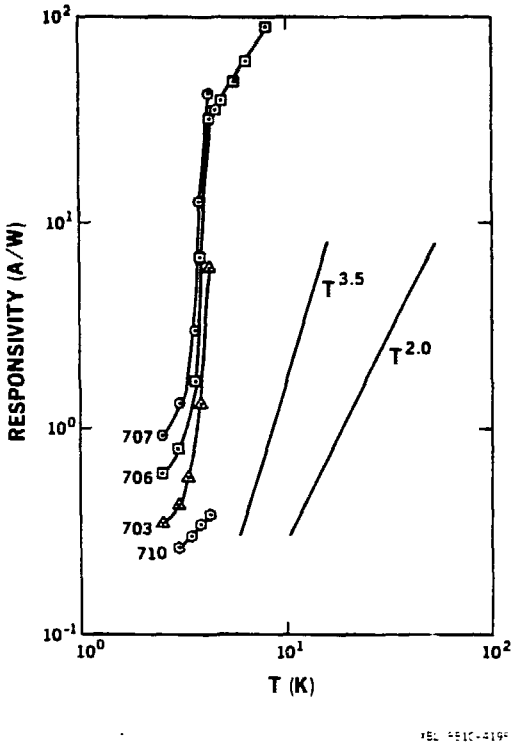

Figure 18
Responsivity as a function of temperature for four Ge:Be detectors.

to theory is only possible in Si at high electric fields where the field effect eliminates the contribution of the higher excited states to the recombination process. In Ge far-IR detectors, this temperature dependence of σ cannot be neglected, since detectors are operated at low fields and low temperatures where trapping by the excited states is important. In contrast, the Poole-Frankle effect, which is included in the Si modeling, is less important for the low field Ge case.

Measurements of the temperature dependence of the capture cross section for T<4.2 K are not extensive. The data collected by Abakumov indicates that the T^{-3} dependence holds to below 3.0 K. For this

reason, a $T^{-2.5}$ dependence for the product $\langle v \rangle \sigma$ was assumed in the modeling of the Ge:Be responsivity.

Figure 19 compares the results of the numerical calculation of responsivity as a function of temperature with the experimental data for a Ge:Be detector. The conversion from dp/dQ to measured responsivity values is given by:

$$R\ (A/W) = \frac{AVe\mu}{Lh\pi} \frac{dp}{dQ} \qquad (3.5)$$

where A is the detector area, V is the applied bias, and L is the intercontact distance.

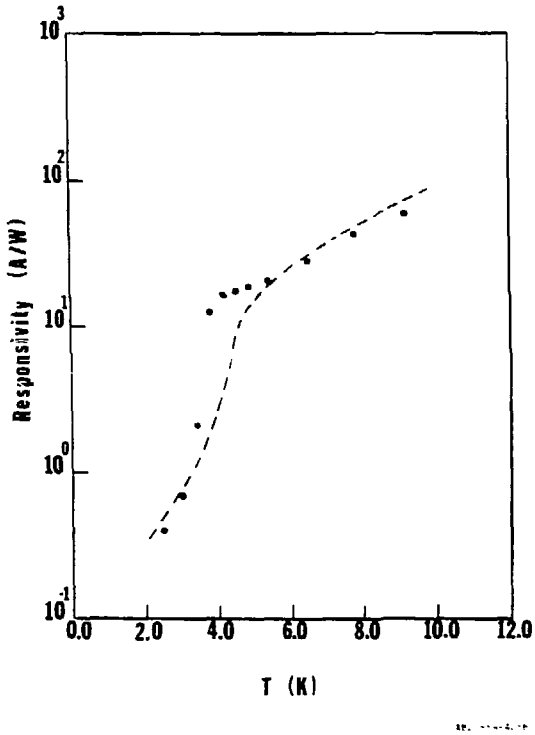

Figure 19
Responsivity as a function of temperature for a closely compensated Ge:Be detector. The dashed line is the theoretically calculated curve.

It is important to note that there are no fitting parameters in the calculation and that absolute values for responsivity, as well as the shape of the curve are calculated. The deviation of experiment from theory in determining the exact temperature at which the strong lifetime increase occurs may be due to uncertainty in the calculation of the photon flux or in the magnitude of the capture cross section. The temperature of the device in the range from 2.0 to 4.2 K is believed to be accurately known to within 0.05 K.

3.3 Methods for Obtaining Close Compensation

In order to obtain the very high values of responsivity predicted for the exact compensation of shallow levels, it is necessary to be able to control the concentrations of the shallow donors and acceptors. The difficulty of this is apparent, since, at least for the case of high purity material, these levels are present only as residual impurities. There are two methods that are commonly used to closely compensate residual shallow impurities. The first, which was used in the work on the Si:In detectors, is neutron transmutation doping (NTD) (37). This technique produces a uniform distribution of phosphorus dopant in Si, and the concentration is proportional to the total neutron fluence incident upon the material. NTD could also be used in Ge although the process would be less efficient since the transmutation of Ge leads to the production of both donors and acceptors with a fixed compensation ratio of $N_D/N_A \sim 0.4$ (38). Because more shallow acceptors are produced in the case of Ge, one can only compensate crystals which initially have net donor concentrations. A second approach is to determine the net residual impurity concentration under routine crystal growth conditions and then

counterdope in the melt to attempt to compensate to the required level. This is a less controlled method, but can be done if high purity growth conditions lead to reproducible results.

A third approach, however, which has been investigated experimentally here for the first time is to control the shallow level compensation by controlling the concentration of several novel shallow acceptor complexes. The following sections will describe the discovery and characterization of these centers, their annealing behavior, and the effect on free carrier lifetime and photoconductive responsivity.

3.3.1 Be-H and Zn-H Complexes

A number of hydrogen-related complexes have been observed and modeled in high purity germanium (39). Impurity-related complexes such as Zn-Li in Ge and Be-Li in Si have also been observed (40,41). In the course of this work, two new shallow acceptor complexes, denoted A(Zn,H) and A(Be,H), have been discovered in Be and Zn-doped material grown for photoconductor applications (42,43). These centers were first observed by R. E. McMurray Jr. in the process of characterizing these materials using photothermal ionization spectrocopy (PTIS).

The first evidence for the Zn-H complex is shown in the PTIS spectra of Figure 20, where a new set of lines with spacing identical to the ones of shallow acceptors, not associated with any known complex or elemental impurity, can be seen. The ground state of the complex is at E_v+ 12.53 meV. The association of this complex with hydrogen is supported by the absence of these lines in a Zn-doped crystal grown under a nitrogen atmosphere. In this group II - hydrogen complex, the hydrogen appears to act as a donor and give its electron to the complex, changing a double

acceptor into a single shallow acceptor. This is interesting because hydrogen has previously been shown to behave in the opposite way. It binds an extra electron in an empty orbital in the cases of D(H,O), A(H,C), and A(H,Si) (39).

A Be-doped crystal was grown under hydrogen in order to look for evidence of an analogous Be-H complex. Figure 21 shows the resulting

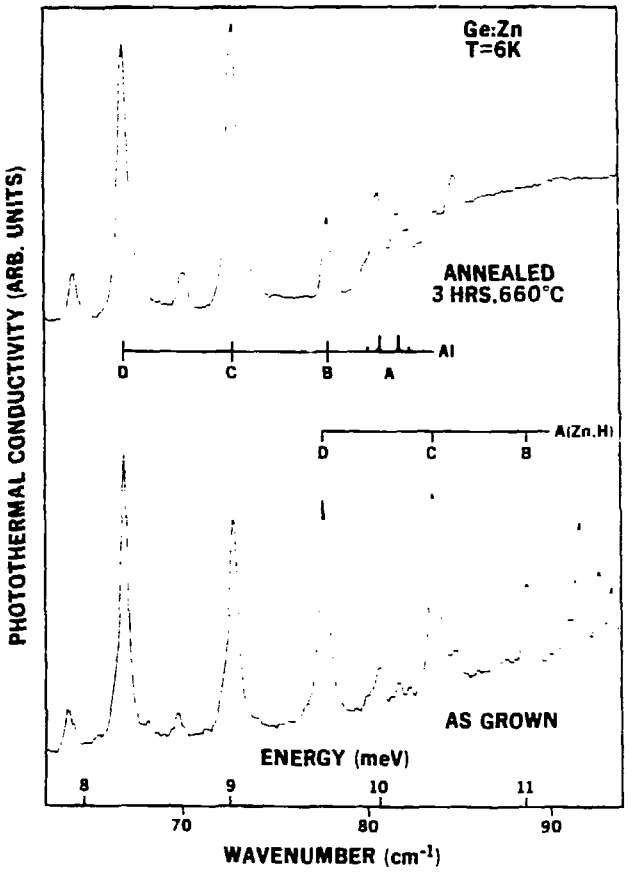

Figure 20
PTIS spectra at T = 6 K

spectra, indicating two new sets of lines with ground state energies of 11.29 and 10.79 meV which are attributed to a Be-H complex with a split ground state. This center was observed in both H_2 and D_2 grown material, although no isotope shift could be detected.

Further evidence for the existence and identification of these complexes has been given by variable temperature Hall effect data. The concentration of these complexes can be reduced by thermal annealing and the change in concentration as a function of time and temperature can be

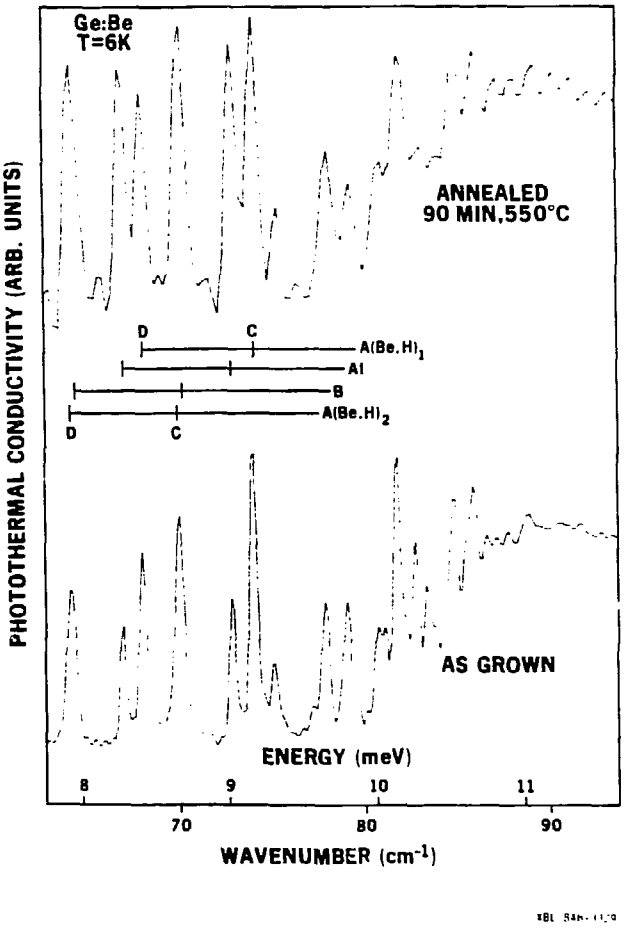

Figure 21
PTIS spectra at T = 6 K

monitored with Hall effect measurements. This is shown for both the Be-H and Zn-H cases in Figures 22 and 23. In both cases, the crystal charge was prepared such that $N_D > N_{A(elemetal)}$, although initially $N_{A(elemental)} + N_{A(complex)} > N_D$. One observes in this material first a decrease in the net shallow acceptor concentration and then a shift from undercompensation to overcompensation of shallow levels. Note that the complexes are initially present in a concentration of about 1 percent of the primary dopant. This is a high concentration compared to the concentrations of other known complexes in Ge, but it is not high enough to cause any measurable change in the elemental Be concentration during the annealing process.

The crystal charges used to grow these crystals were summarized in Table 1. It was necessary to counterdope the Be crystals to obtain the $N_D > N_A$ condition. In general, B and Al are present in higher concentation than the compensating donors in the Be doped crystals. This is consistent with the observation that all the high purity Ge crystals grown directly from a carbon susceptor are p-type. In the Ge:Zn case, the $N_D > N_A$ condition was obtained in one crystal without counterdoping. This crystal was grown from a silica crucible which releases much smaller concentrations of Al and B. It is also possible that the Ge:Zn master alloy itself was a source of n-type impurities.

3.3.2 Annealing Behavior of Be-H and Zn-H Complexes

The concentration data obtained from the Hall effect measurements can be used to determine the rate equation for the annealing of the H-related complexes. As a model for the annealing of the complexes, we will assume

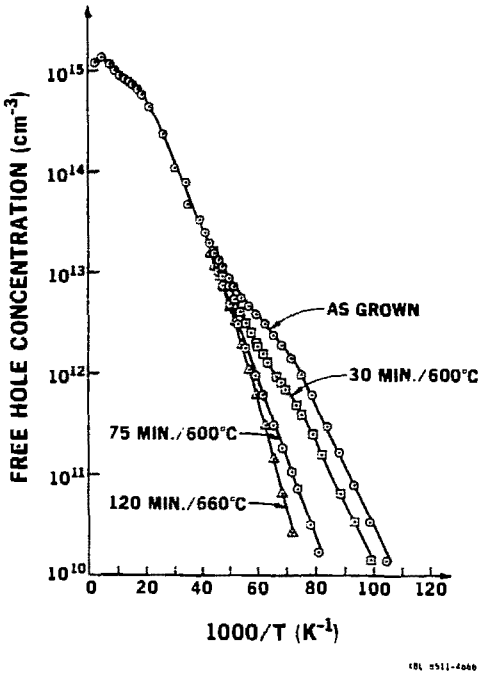

Figure 22
Carrier concentration as a function of inverse temperature showing effect of annealing on compensation of shallow levels for Ge:Be

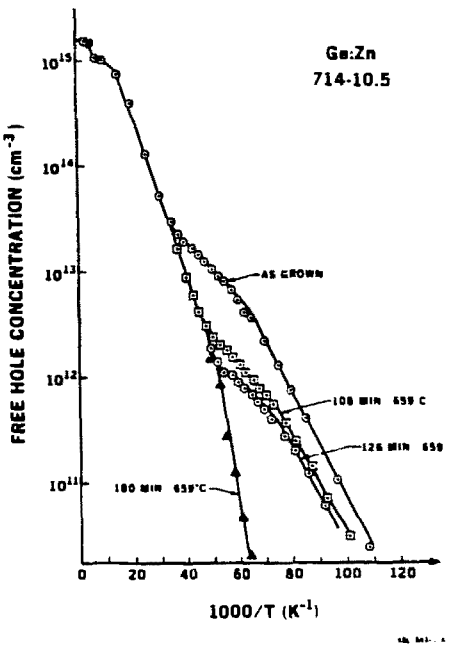

Figure 23
Carrier concentration as a function of inverse temperature showing effect of annealing on compensation of shallow levels for Ge:Zn

a dissociation of the Zn-H or Be-H, followed by out-diffusion of the free H. The temperatures required to see a measurable decrease in concentration after a one hour anneal were ~650°C for Zn-H and ~550°C for Be-H. At these temperatures, a calculation of the out-diffusion of H from a 1.0 mm Ge slab indicates that 99% of the H will have left after 1 hr at 600°C (44). Using this result, we assume that the dissociation of the complex is the rate-limiting step for thin samples. This assumption is supported by the fact that the Be-H and Zn-H complexes begin to anneal at different temperatures, indicating that the rate-limiting step is dependent on the binding energy of the complex rather than the H diffusion.

The decrease in complex concentration as a function of time for two different annealing temperatures is shown for the Zn case in Figure 25. If one assumes a first order reaction for the rate equation

$$n = N_0 \exp\left(-t(\nu \exp(-E/kT))\right) \qquad (3.6)$$

the following values are obtained for the prefactor ν and the dissociation energy E_d:

Zn-H	$\nu = 3\times10^{12}\ s^{-1}$	$E_D = 3.0 \pm 0.3$ eV
Be-H	$\nu = 3\times10^{8}\ s^{-1}$	$E_D = 2.1 \pm 0.6$ eV

The values of the dissociation energy for these complexes are significantly higher than for other H-related complexes. They are consistent, however, with the observation that Cu complexes in Ge are stable to temperatures in excess of 700°C (45).

The development of a microscopic model for this system relies heavily upon symmetry data obtained from piezospectroscopy. Preliminary results indicate that the Be-H center is stress-insensitive, i.e., the ground

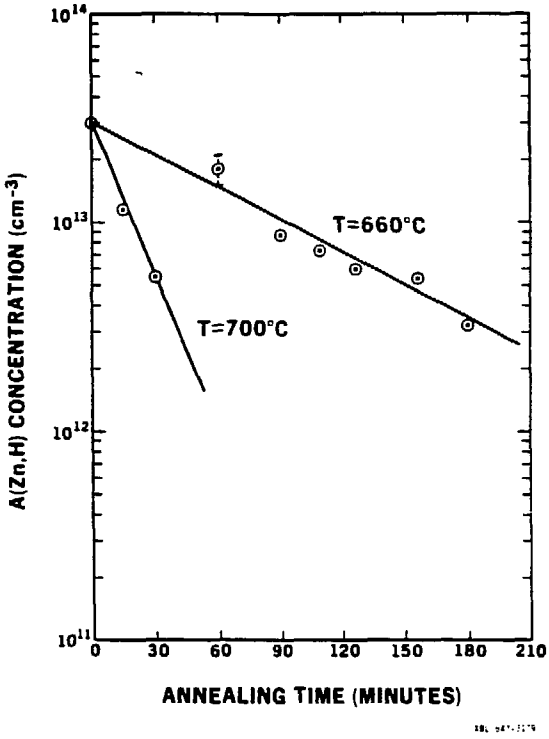

Figure 25
A(Zn,H) concentration as a function of annealing time for T=660°C and 700°C

state does not split under stress, while the Zn-H center splits under conditions which indicate an orientation of the defect along the [111] axis. Models for tetrahedrally symmetric, hydrogen-related centers, with a hydrogen tunneling in the vicinity of a substitutional impurity have been proposed for a number of centers (41). The observation of a Zn-H center with a [111] orientation may be indicative of a different case in which the H is locked in a fixed position. Work on these models is in progress, with the goal being to propose a comprehensive model to describe the behavior of Be-H, Zn-H, and Cu-H complexes.

3.4 Effect of Compensation on Free Carrier Lifetime and Responsivity

Although models have been proposed and used to fit several experimental cases of the temperature dependence of responsivity for Si:In, no systematic study has yet been done to show the increase in free carrier lifetime with increasing degree of compensation of the shallow levels. This can be done using the photo-Hall technique to measure free carrier lifetime as a function of temperature, as described in Chapter 2. The difficulty in carrying out such an experiment has previously been that no means was readily available for changing the compensation in a sensitive enough manner near the point of exact compensation.

The annealing of the Be-H complex was used to obtain several samples with increasing degree of compensation. These samples are labeled A through C in Figure 26, which shows the Hall effect data in thermal equilibrium and the photo-Hall data in the presence of a constant photon flux. The flux source was a 300 K blackbody which entered the sample chamber through a small (d = 0.2 mm) aperture. In Figure 27, the region of the lifetime increase has been expanded and plotted as log (p) versus log (T). The increasing magnitude of the lifetime increase and the strong deviation from the power law in T as the degree of compensation is increased are clearly visible.

A second example of the effect of shallow level compensation on photoconductor responsivity was observed when photoconductors were produced from different sections along the length of a crystal which became more closely compensated with increasing distance from the seed end. Hall effect results for four slices are compiled in Figure 28. One sees that the shallow levels in the crystal actually form a junction at a certain distance from the seed, so that $N_{A(shallow)} > N_D$ at the seed

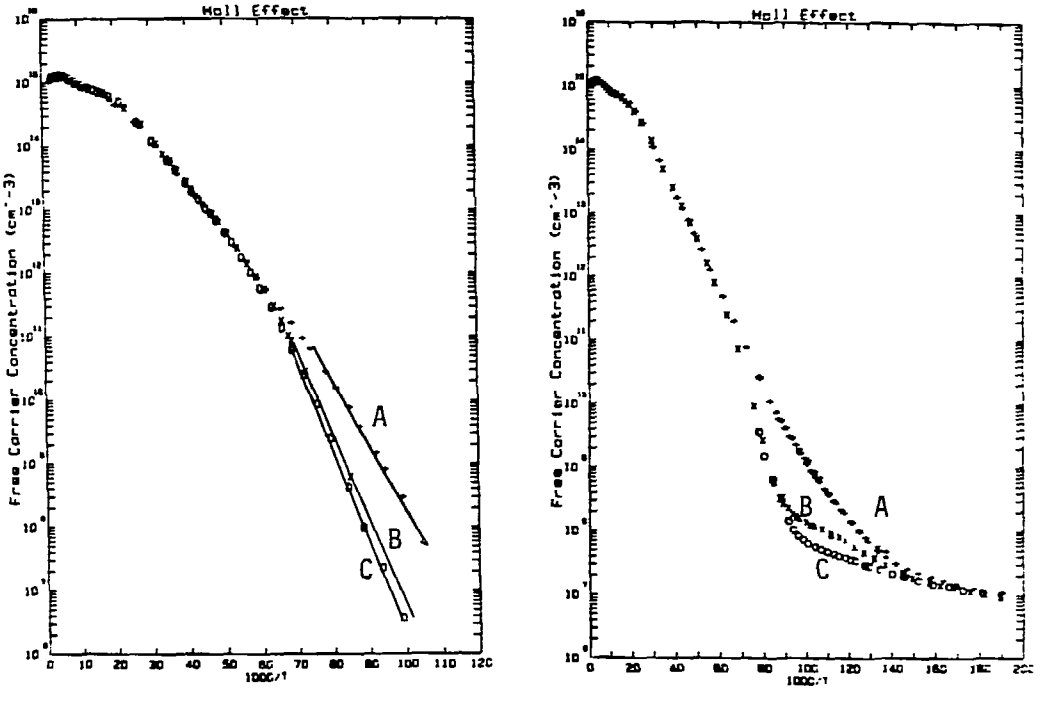

Figure 26
Hall effect and Photo-Hall effect measurements of closely compensated Ge:Be

A Ge:Be 728-4.3 Annealed 75 minutes at 600°C
B Ge:Be 728-4.3 Annealed 90 minutes at 660°C
C Ge:Be 728-4.3 Annealed 120 minutes at 660°C

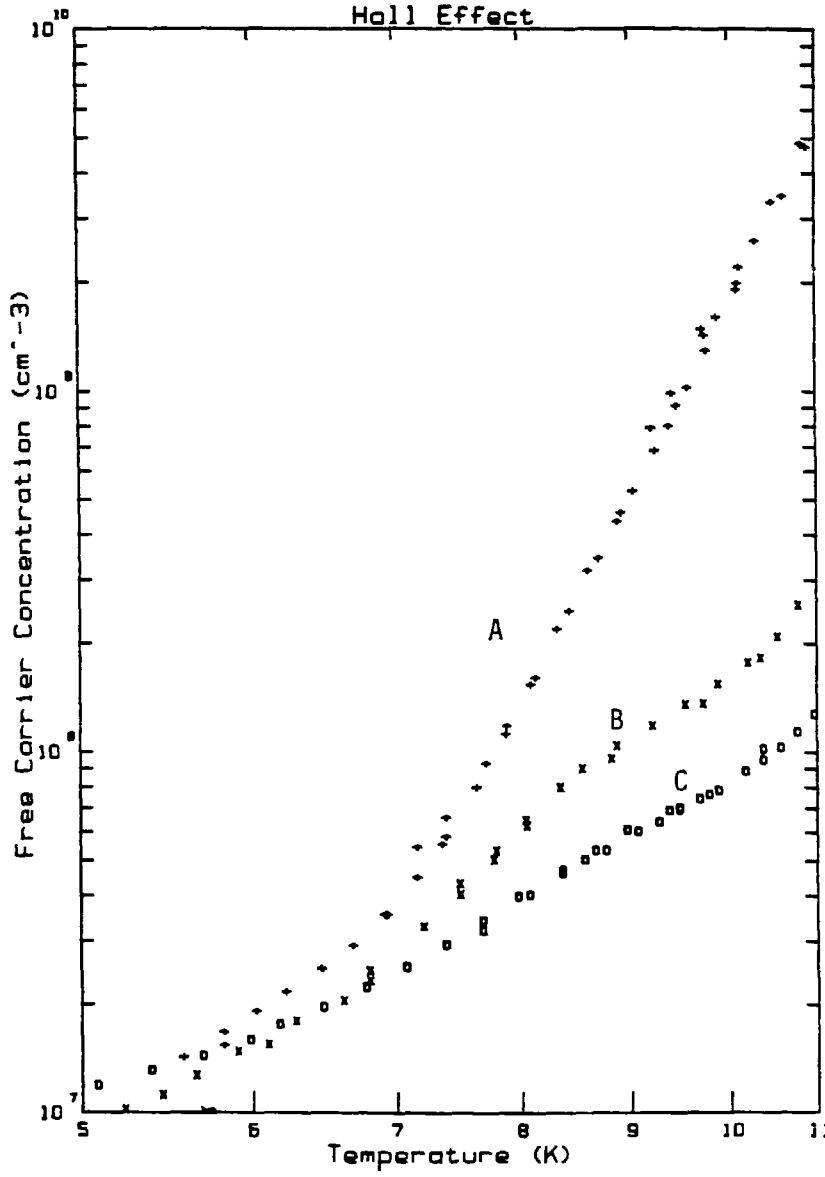

Figure 27
Free carrier concentration as a function of temperature showing lifetime increase in closely compensated material

end, while $N_D > N_{A(shallow)}$ at the tail. Responsivity values as a function of temperature for some of the detectors are plotted in Figure 29, showing that the increase in responsivity corresponds to an increasing degree of compensation.

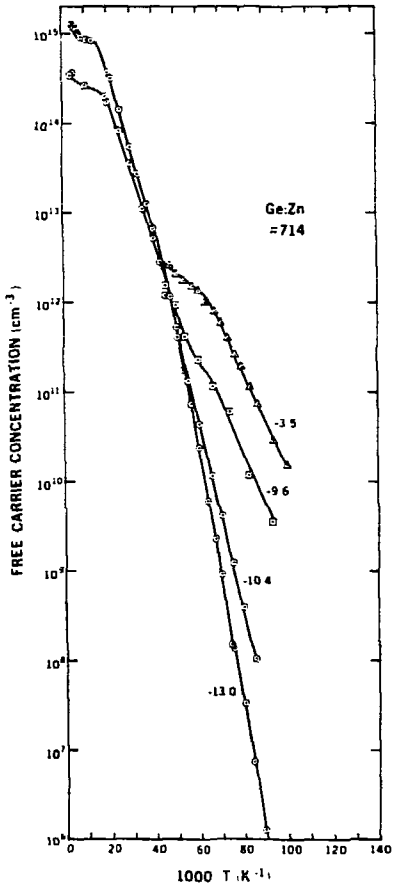

Figure 28
Hall effect data for Ge:Zn samples from crystal 714
Labels indicate distance in cm from the seed end

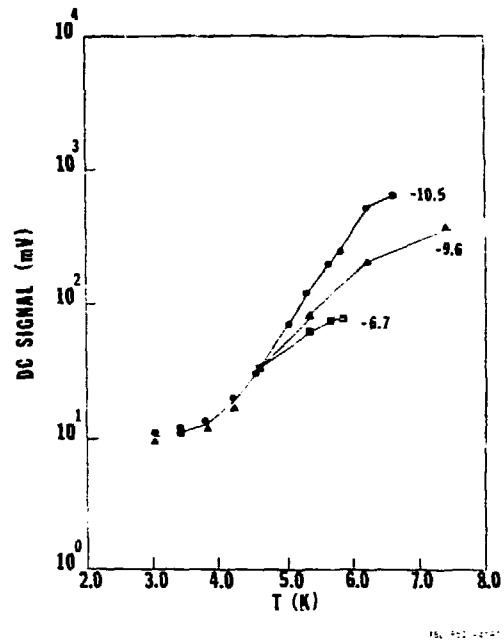

Figure 29
Signal size as a function of temperature for Ge:Zn detectors with increasing degree of compensation of shallow levels

Another feature is evident in the freeze-out data for the closely compensated case. Near the junction, the freeze-out slope does not show the behavior typical of either a clearly under- or over-compensated case. Instead, the sample continues to freeze-out with an intermediate slope of ~15 meV down to very small values of carrier concentration. Since it is unlikely that the compensation is really as close as 1 part in 10^4 (10^8 out of 10^{12} cm^{-3}), some other mechanism must affect the concentration as measured by Hall effect. This behavior has been observed a number of times in samples near junction. In all cases, however, these samples were taken from the tail end of the crystal,

raising the possibility that there may be dislocation effects which affect the Fermi level or provide a conduction path which affects the measured Hall voltage at high values of sample resistivity. Striations will also become important when the materials are very closely compensated. In close analogy, it is known that ultra-pure silicon often does not show either p-type or n-type conduction at low temperatures. It is assumed that the material consists of islands of both types.

3.5 Summary of Material Parameters for Multi-level Photoconductors

Because of the significant role that residual shallow levels play in determining the responsivity and dark current in a multi-level system, the selection of optimized material for detectors such as Ge:Be or Si:Ga requires full characterization of the material with regard to both primary and residual dopants. In addition to the standard selection criteria for material properties for photoconductors, one must also determine, based on the operating temperature of a device and the background flux levels expected during observation, whether enhanced responsivity due to close compensation is a desirable goal. In cases where the detectors are expected to be photon noise limited, high responsivity is perhaps helpful in reducing the need for signal amplification but will not lead to improved signal to noise performance. If, however, the limiting noise source is amplifier noise or dark current noise, then improved responsivity may improve the detection limit. An attempt has been made, in Figure 30, to consider the factors involved in material selection of multi-level materials for low background astronomy.

Finally, an example will illustrate the use of Figure 30. Consider an indium doped Si photoconductor being developed for a low background

Material Selection:
Shallow Level Compensation*

$N_D >> N_A$	$N_D > N_A$	$N_D < N_A$	$N_D << N_A$
Highest ρ	High ρ	Lower ρ	Lowest ρ
Lowest dark current	Low dark current	Higher dark current	High dark current
$R \alpha \frac{1}{N_D}$	$R \alpha \frac{1}{N_D}$ for $T < T_c$		$R \alpha \frac{1}{N_D + p}$
	$R \alpha \exp(-E_B/kT)$ for $T > T_c$		
	where $T_c = \frac{E_A}{k \ln(\frac{Nv}{gp})}$		

* N_A refers to residual shallow acceptors and does not include the primary dopant (Be in Ge, In in Si, etc.)

Figure 30

($\dot{p} \sim 10^8$ photons/sec) space application on a focal plane at T=3.0 K. Indium doped silicon is grown using the floating-zone technique and generally has a net shallow acceptor concentration due to the presence of residual boron unless intentionally counterdoped. Boron is hard to remove from silicon because it has a segregation coefficient (k_s=0.8) very close to unity. Perhaps, because of the low background and small signals, one desires to have as high a responsivity as possible in order to overcome some fixed level of background noise, such as electronics

related noise. Finally, suppose the resistivity in the as-grown case ($N_A > N_D$) is sufficiently high at 3.0 K to eliminate measurable dark current noise.

To determine if one should counterdope (i.e., add donors) to attempt to achieve $N_A \approx N_D$ and high responsivity, one should calculate the temperature at which the lifetime increase due to exact compensation would occur. In this case, for $p=\dot{p}\,\tau = 10^3$ cm^{-3}, and E=45 meV for boron, T_c = 17 K. Therefore, the focal plane temperature is so far below T_c that the responsivity will be given by

$$R \sim (N_D)^{-1} \qquad (3.7)$$

and the addition of n-type dopants would only increase N_D and be detrimental rather than beneficial in achieving the goal of high responsivity. If, however, the resistivity of the as-grown material was not high enough to eliminate dark current effects, then counterdoping would be required, with some sacrifice in responsivity. Analysis of a similar case in Ge might lead to other conclusions because the shallower levels in Ge means that enhanced responsivity can be achieved at lower temperature for a given flux.

Chapter 4 Transient Responses in Ge:Be and Ge:Zn Photoconductors

The study of the transient response of extrinsic photoconductors to cnanges in photon flux has traditionally been the most challenging issue in the field. Under conditions of very low photon fluxes, where carrier densities can be as low as 10 cm^{-3}, extrinsic photoconductors are well known for exhibiting transient behavior characterized by long time constants, memory effects, and highly non-linear behavior. Due to the variety of different phenomena that have been observed, as well as the large number of parameters involved and the analytical intractability of the equations describing the non-steady-state, very little work has been done to characterize or model transient behavior without recourse to empirical description. Understanding transient phenomena, however, remains an extremely important goal because the application of photoconductors dictates that they are most often used in a transient fashion. Low background astronomy observations are done using low frequency chopping to allow for background subtraction and absolute calibration of the size of signals. Transient behavior that is characterized by long time constants limits the speed of the detector, extends the required observing time for a given sensitivity, and limits the detector ac responsivity.

Ge:Be and Ge:Zn detectors have been shown to display, under certain conditions, a transient response that is characterized by time constants on the order of seconds. In this section, the existing models for the transient response of extrinsic photoconductors will be reviewed and found to be inadequate to explain the observed behavior. An extensive study of the transient behavior, as a function of temperature, bias, photon flux, detector geometry, and materials parameters will be presented. Finally, some theoretical modeling of transient phenomena which includes a realistic model of near-contact space-charge-dependent behavior will be presented.

4.1 The Space Charge Neutral Model

A simple model for the transient response of an extrinsic photoconductor can be derived for low background operation if one assumes a space charge neutral detector and neglects all contact effects. In this case, the rate equation for the change in free holes is given by

$$\frac{dp}{dt} = \underbrace{Q}_{\text{optical generation}} + \underbrace{N_v \langle v \rangle \exp \frac{E^f - E^v}{(kT)}}_{\text{thermal generation}} - \underbrace{\langle v \rangle \sigma p (N_D + p)}_{\text{recombination}} \qquad (4.1)$$

where Q is the photon flux rate, N_v is the valence band density of states, $\langle v \rangle$ is the average thermal velocity, $E^f - E^v$ is the Fermi level referenced to the valence band, and σ is the recombination cross section. This expresssion assumes that optical and thermal generation and cascade capture recombination are the dominant processes in the material, neglecting other effects such as impact ionization, radiative recombination, and Auger recombination. This is a very good approximation for low background photoconductors operated at fields below the breakdown field.

This rate equation can be written as

$$dp/dt = g - p/\tau \qquad (4.2)$$

where g is the sum of all generation terms and $\tau = (\sigma v N_D)^{-1}$ since $N_D >> p$ for low background flux. If we increse g by an amount Δg then

$$d\Delta p/dt = \Delta g - \Delta p/\tau \qquad (4.3)$$

For the case where Δg arrives as a step pulse ($\Delta g = 0$ for $t < t_o$, Δg=constant for $t > t_o$) then

$$\Delta p = \Delta g \tau (1 - \exp(-t/\tau)) \qquad (4.4)$$

Since for low background work, τ is not generally a function of the photon flux, this model predicts that the transient response should be

given by the lifetime of free carriers in the device and should be symmetric with regard to growth or decay for small changes in photon flux. It is from this model for transient response that one derives the standard relationship between lifetime, compensation, and detector bandwidth.

4.2 Effects of Space Charge and Non-linear Behavior

Although it is of general use in predicting first order behavior, the simple linear model for the space charge neutral photoconductor fails to explain many of the phenomena which are observed during operation. This is not surprising since photoconductors are actually non-linear devices which are not space-charge neutral. Non-linear behavior arises because the coefficients for recombination or impact ionization processes are actually strong functions of electric field. Space-charge regions exist near both contacts and may, under some circumstances, exist in the bulk as well.

One of the earliest models for space charge related effects on transient behavior was proposed by Williams in 1969 (46). He observed a slow component ($\tau >> \tau_{lifetime}$) in the response of Ge:Hg under conditions where the photoconductive gain was greater than unity. This was attributed to the "sweep-out" of carriers generated by external illumination, leading to a space charge region in the device. Since the relaxation of the space charge was theoretically shown to occur with a time constant of $\rho\varepsilon\varepsilon_0$ (the product of resistivity and the dielectric constant), the term dielectric relaxation has since been applied to this phenomena. It is important to understand the predictions and limitations of this theory, since it is often improperly invoked as an explanation for any slow transient response observed in extrinsic photoconductors.

The theory of carrier sweep-out and dielectric relaxation assumes a restrictive boundary condition ($\Delta p=0$ at the anode) so that no free carriers are immediately available for injection. In this case, when a pulse of light is incident upon the device, free carriers Δp will be produced and will move toward the cathode under the effect of the applied field. Near the anode, a concentration $\Delta N_A^- = \Delta p$ of ionized acceptors will be left. This space charge layer will produce an electric field gradient, i.e.,

$$dE/dx = -e\Delta N_a^-/\epsilon\epsilon_0 \qquad (4.5)$$

which integrates to

$$\Delta E(x) = -eN_a^-(L-x)/\epsilon\epsilon_0. \qquad (4.6)$$

The continuity equation is given by

$$d\Delta N_a^-/dt = (1/e)dJ/dx \qquad (4.7)$$

$$= \mu p_0 dE/dx \text{ for } J = e\mu p_0 E$$

$$= -\mu p_0 q\Delta N_a^-/\epsilon\epsilon_0$$

Integrating, one obtains

$$\Delta N_a^-(t) = \Delta N_0^- \exp(-t/\tau) \quad \text{where} \quad \tau = \epsilon\epsilon_0/(\mu p_0 e) = \epsilon\epsilon_0\rho_0 \qquad (4.8)$$

Thus, the space charge region is neutralized with a response time proportional to the detector resistivity.

This theory has been cited extensively when long time constants are observed in extrinsic photoconductors. Its greatest success has been in explaining the rolloff of photoconductive gain as a function of frequency for high resistivity detectors with the more advanced forms of the theory (47,48). However, there are several limitations to the model. The most important is the assumption of a boundary condition of $\Delta p=0$ at the anode. This means that no free holes are readily available for injection at the contact. There is no firm justification for this, especially in the case

of an ohmic, ion-implanted contact which serves as a reservoir for free carriers even at very low temperatures. A restrictive boundary condition is a requirement for sweep-out to occur, and the fact that some behaviors are well described by the dielectric relaxation theory indicates that contact behavior may not be perfectly ideal. This will be discussed further in Chapter 5. However, the boundary condition that $\Delta p=0$ at the contact seems to be more mathematically appealing than realistically valid.

4.3 Effects of Contact Behavior

In 1959 Lampert and Rose published a phenomenological analysis of the transient behavior of ohmic contacts (49). They proposed that the response time of a photoconductor for current transients could, under certain circumstances, be determined by the readjustment of the space charge barrier at the contact. Figure 31 shows a schematic view of the change that must occur in the injecting contact for an increase in current through the solid.

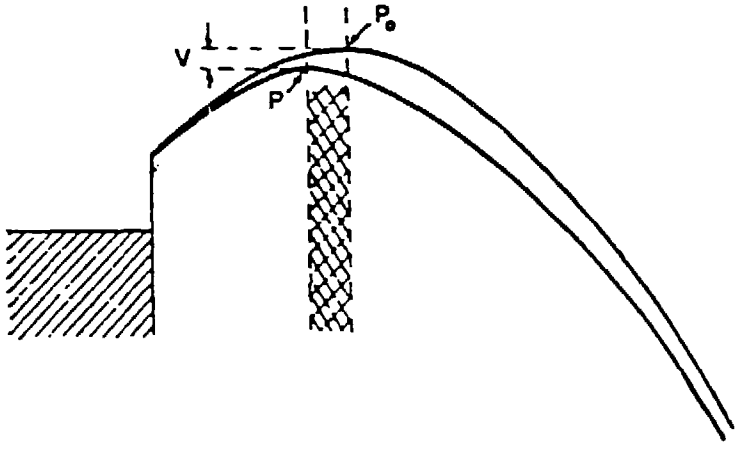

Figure 31
Response of an ohmic contact to an increase in bulk conductivity (Ref. 49)

By calculating the required change in the space charge distribution to lower the energy maximum, the authors arrived at the following expression for the contact "rise time":

$$\tau_c = \frac{A}{F}\left(\frac{\epsilon k T N_T}{e^2}\right)^{1/2} \qquad (4.9)$$

where A is the contact area (cm^2), F is the change in the carrier generation rate (#/sec), and N_T is the concentration of space charge (cm^{-3}) which is assumed to be constant near the contact. For a 1 mm^2 device with a $\Delta Q = 1x10^8$ p/sec and $N_T = 10^{12}$ cm^{-3} at 4.2 K, $\tau_c = 6.2x10^{-3}$ seconds.

The transient response predicted by this model is symmetric with respect to rise time and decay time because it depends only on the change in the excitation rate, ΔF. The important material parameter is the space charge, N_T, within approximately one Debye length of the energy maximum. This model will be discussed more extensively in Chapters 4 and 5.

4.4 Transient Behavior in Ge:Be and Ge:Zn: Experimental

The transient response of Ge:Be and Ge:Zn detectors to a step increase in photon flux was studied over a wide range of parameters. The change in signal was caused by manually moving a reflecting gold plated shutter which switched the detector field of view from the 77 to the 300 K blackbody source. The flux levels and flux change are given in Table 5. It is clear that, since $\Delta p > p_0$, this is not a case of small signal response. It is an experimental condition, however, which does correspond to what the detectors often see in practice. The speed at which the shutter was opened was approximately 20 msec. Although this is

TABLE 5

Photon Flux Levels for Transient Measurements

Detector	Ge:Be	Ge:Zn
λ (μm)	42	36
Background flux(p/s)	1.5×10^8	1.5×10^8
Bkgr. + signal (p/s)	8.9×10^8	1.1×10^9
Signal Δ (p/s)	7.4×10^8	9.2×10^8

a long time relative to the free carrier lifetime, we will see that it is very short compared to the time constants which were observed.

The most interesting transient response which was observed, which will be the subject of most of the experimental characterization, is illustrated in Figure 32 for Ge:Zn and Figure 33 for Ge:Be. A slow component is observed which increases in magnitude with increasing device temperature. The time constant of the response, assumed to be the point where the slow component attains 63% of its full value, ranges from <0.1 sec (the shortest time which could be detected experimentally) to greater than 5 seconds for Ge:Zn and from <0.1 second to 2 seconds for Ge:Be. Additional features of the response can be observed by considering the compiled data in Figure 34, which indicates clearly that the photoresponse is composed of both a fast and a slow component. The magnitude of the fast component increases only slightly with increasing temperature, while the slow component increases must faster so that, at certain temperatures, it appears to fully dominate the photoconductive response (see Figure 33e).

The time constant of the slow component decreases with increasing temperature and has been plotted as a function of inverse temperature in Figure 35. The activation energy associated with the slope is

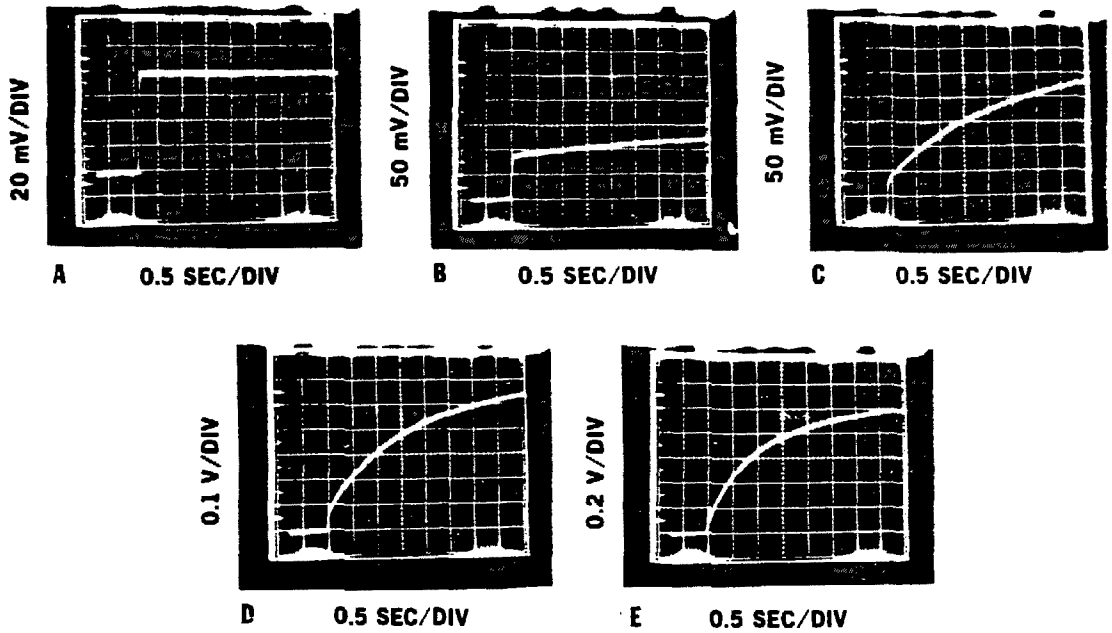

Figure 32
Transient response of Ge:Zn detector at
T = a) 5.2 K b) 6.3 K c) 7.3 K d) 8.4 K and e) 9.0 K

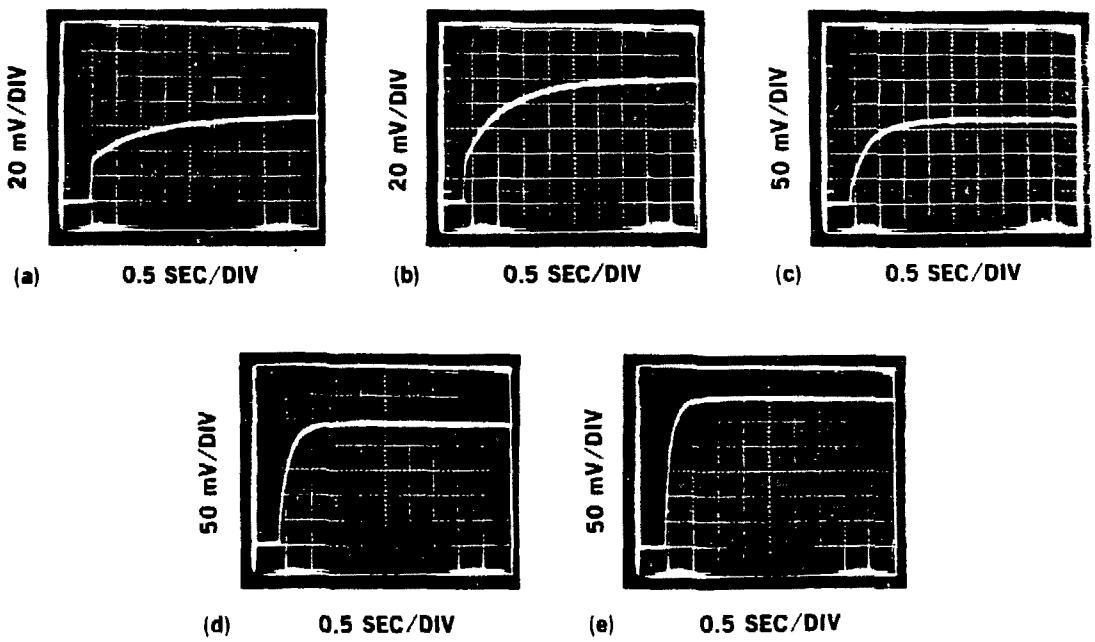

Figure 33
Transient response of a Ge:Be detector at
T = a) 2.5 K b) 2.6 K c) 2.7 K d) 2.8 K and e) 2.9 K

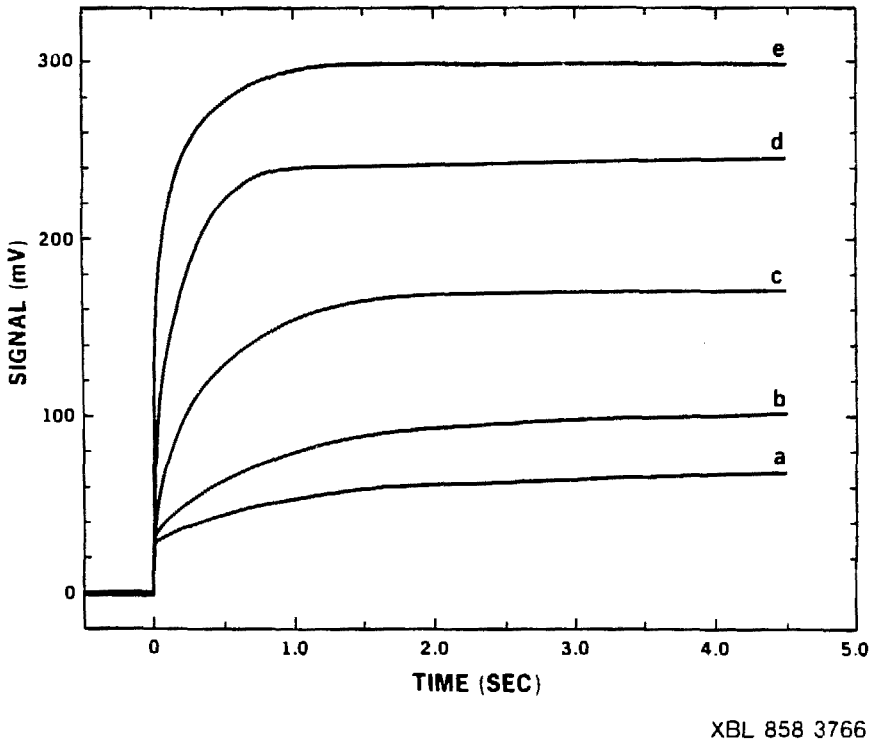

Figure 34
Compiled data from Figure 33 showing the effect of increasing temperature on signal size

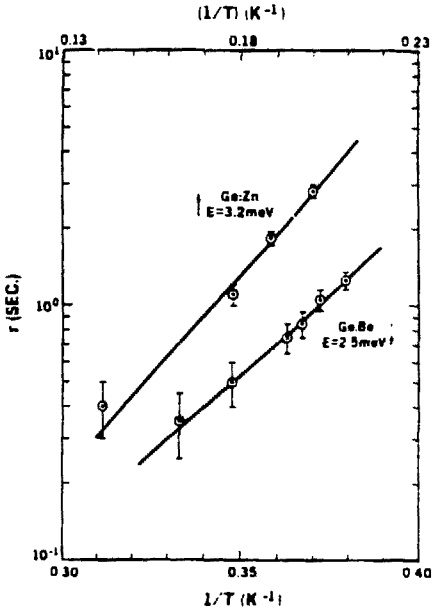

Figure 35
Time constant of the slow component as a function of inverse temperature

approximately 2.5 meV for the Be case and 3.2 meV for Ge:Zn. This is an interesting result, since this energy does not correspond to any of the ionization energies of the known elemental dopants in the material. Nevertheless, these activation energies have been measured several times and have been found to be relatively insensitive to changes in detector bias or material doping, differing only by several tenths of an meV for different devices.

Because an increase in detector temperature necessarily implies an increase in free hole concentration (due either to increased thermal generation or to increased lifetime), it was important to determine if the faster time constant with increasing temperature was actually due to increasing lattice temperature or the resultant increase in free hole concentration. In order to separate these two effects, a separate blackbody photon source (a 1 kΩ resistor) was placed in the dewar within the field of view of the detector. The temperature of this source could be varied externally. Temperature changes at a constant flux could then be compared to the effect of photon background changes at a constant temperature, with both effects causing the same change in free hole concentration in the device.

The results of this experiment are presented in Figure 36 for a Ge:Be detector. One sees that the decrease in time constant is due to the change in lattice temperature and not to the increase in background hole concentration. The effect of increasing hole concentration is weak, if any, over the measured range. Thus, the time constant is not directly proportional to detector resistivity, an important indication that dielectric relaxation is not determining the transient behavior. Because these initial experiments indicated that this is a different behavior

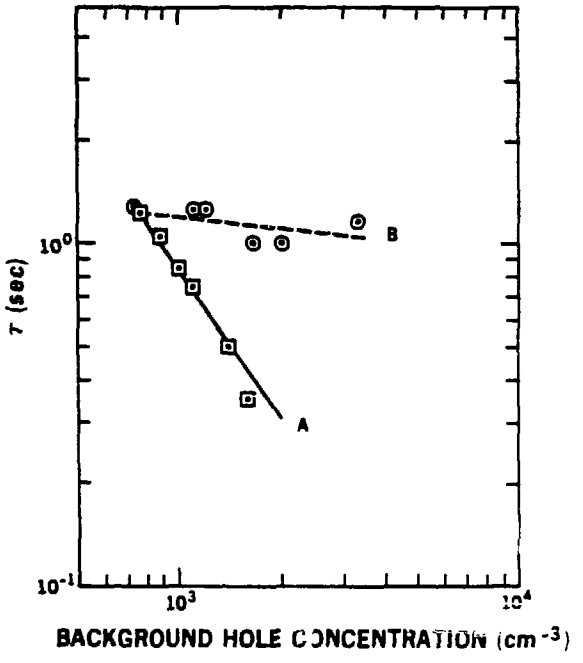

Figure 36
Time constar' for the slow component as a function of background ..le concentration, where the hole concentration was changed by changing A) temperature and B) background flux

which is not predicted by existing theory, it was necessary to establish the effect of the major variables affecting photoconductor performance: temperature, bias, intercontact distance, detector size, and material parameters.

4.4.1 Temperature

The temperature dependence of τ was plotted in an Arrhennius plot in Figure 35. Some additional points should be made in regard to this data. First, the measured range of time constants was limited on the short side to τ >0.1 sec. Faster time constants began to blend with the effects of time constants associated with the opening of the shutter or other roll-off effects in the device and the electronics. At the low temperature end of the range, measurement was limited by the fact that

the slow component became very small with respect to the total signal, so that accurate measurement of its time constant was impossible.

The temperature dependence is replotted in Figure 37 as log(τ) versus log(T). The data fit a straight line, with power dependences of $\sim T^{-9.2}$ for a number of different samples. There is no theoretical basis at this point for expecting the data to be fit by either a power law or an Arrhenius relation in T.

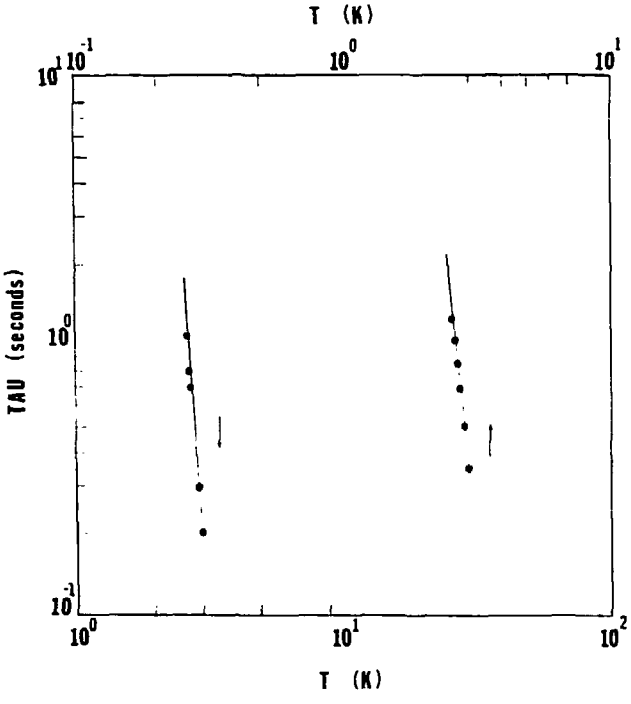

Figure 37
Time constant of the slow component
as a function of detector temperature

The amplitude of both the slow and the fast components is plotted as a function of temperature in Figure 38. The amplitude of the fast component increases much less rapidly with increasing temperature than

the slow component. The power law dependence of the fast component is difficult to determine because of the small temperature range over which it could be distinctly separated from the slow component (i.e., when the slow component is much larger, the fast component cannot be seen. See Figure 33e). However, its temperature dependence is not unlike the power law dependence which would be expected based on the temperature dependence of the free carrier lifetime which was discussed in Chapter 3. The slow component data does not fit a power law in T, but one sees that its temperature dependence is much stronger than that of the fast component.

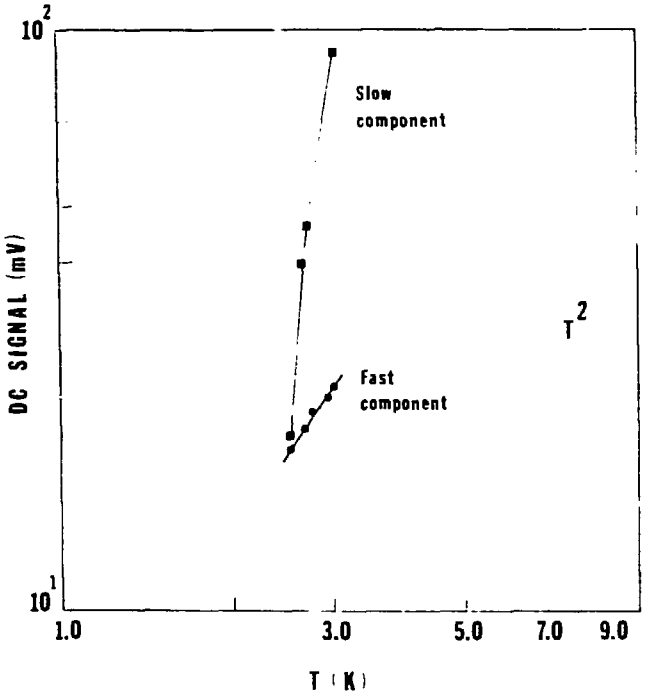

Figure 38
Amplitude of slow and fast components as a function of detector temperature for a Ge:Be detector with slow response

4.4.2 Electric Field

The time constant of the symmetric slow response did not vary with increasing electric field over a range from 1.0 to 6.0 V/cm. The amplitudes of both components as a function of bias are plotted in Figure 39. Both increase with increasing field and there is no evidence of saturation of the fast component, as might be expected for sweep-out mechanisms. The fast component displays a linear response at low fields and approaches a V^2 dependence as the field is increased and carrier heating occurs. This is the standard I-V behavior of extrinsic photoconductors. The slow component, in contrast, displays a superlinear voltage dependence even at low bias.

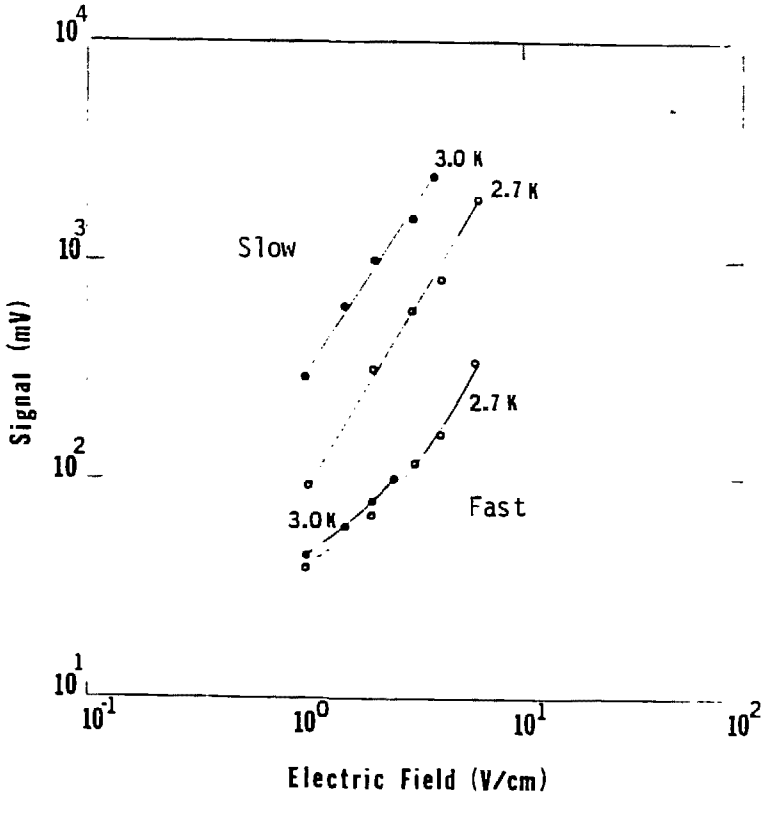

Figure 39
Amplitude of fast and slow component as a function of bias

4.4.3 Intercontact Distance and Contact Area

The effect of the intercontact distance on the slow component response was studied by varying the intercontact distance over a range from 2.5 to 0.2 mm in detectors made from Ge:Be crystal 719-11.6. This has the effect of changing the photconductive gain ($G=\mu\tau E/L$) by a factor of 12.5 if detectors are evaluated at a constant field, V_{bias}/L. The results are tabulated in Table 6 for three different temperatures at a constant field of 1 V/cm. One sees that, at a constant temperature, the time constant of the slow response is independent of photoconductive gain within the measured range.

TABLE 6

Time Constant as a Function of Intercontact Distance

L (mm)	τ* (sec)		
	T = 2.6 K	2.73 K	3.0 K
0.2	1.1	0.4	0.15
1.0	0.9	0.4	0.2
2.5	1.0	0.45	0.10

* all values ± 0.1 second

The time constant of the slow response was also evaluated as a function of contact area to determine the effect of current density through the device for a fixed mobility, lifetime, and photoconductive gain. This was accomplished by testing detectors with varying cross-sectional area (1x1, 1x3, 3x3 mm^2) in similar integrating cavities under the same photon flux. If one assumes that the number of

photons absorbed is constant in the cavity, then the total current must be constant and the current density will scale inversely to detector area.

The effect of increasing contact area is illustrated by the oscilloscope traces in Figure 40. With large area contacts, an additional slow component appeared in the response. This component was more pronounced for the increasing current transient than for the decay, as indicated by Figures 40c and 40d. In Figure 41, theoretical curves based on two exponentials, with $\tau_2 >> \tau_1$ were used to fit the transient reponse. The appearance of an additional slow component is evident by the deviation from the two exponential fit for the large area case. One cannot conclude that the time constant increases with contact area; it simply can no longer be described as:

$$S_t = S_1(1-\exp(t/\tau_1)) + S_2(1-\exp(t/\tau_2))$$

One effect of increasing the detector size under fixed conditions of illumination is that the near-contact illumination becomes increasingly non-uniform. Non-uniform illumination of contacts or of the photoconductor has previously been shown to cause anamolous behavior in extrinsic photoconductors (50). To determine the effect of uniformity of contact illumination, and to determine if the long time constant behavior observed in all the photoconductors was due to that effect, a detector was made in which the contacts were uniformly illuminated. This was done by making a thin detector with contacts on the backside and using front side illumination. This would fully illuminate the front side region and the contact regions. The transient response associated with this detector was included as Figure 41A, and one sees that a long transient response still exists, but that it can be fit very well with a two time constant model.

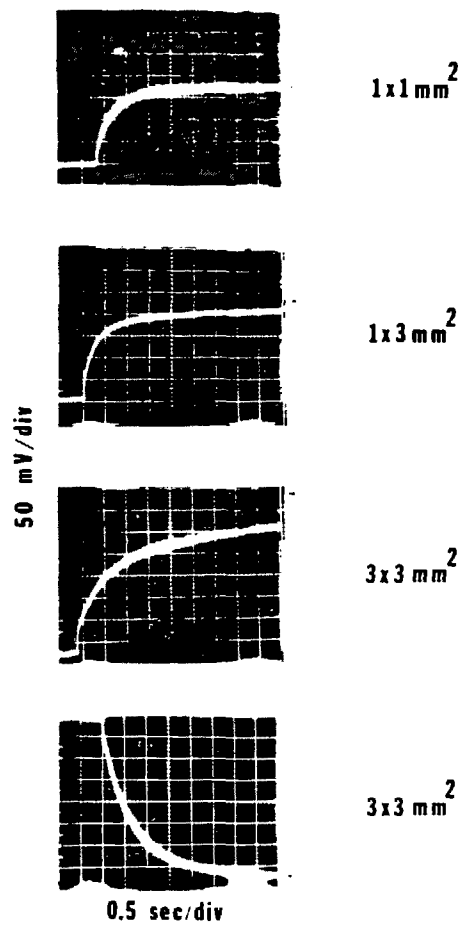

Figure 40
Detector response as a function of device area with constant photon fluence.
Arrows indicate final steady state value of the response. Final picture shows the effect of decreasing the illumination level.

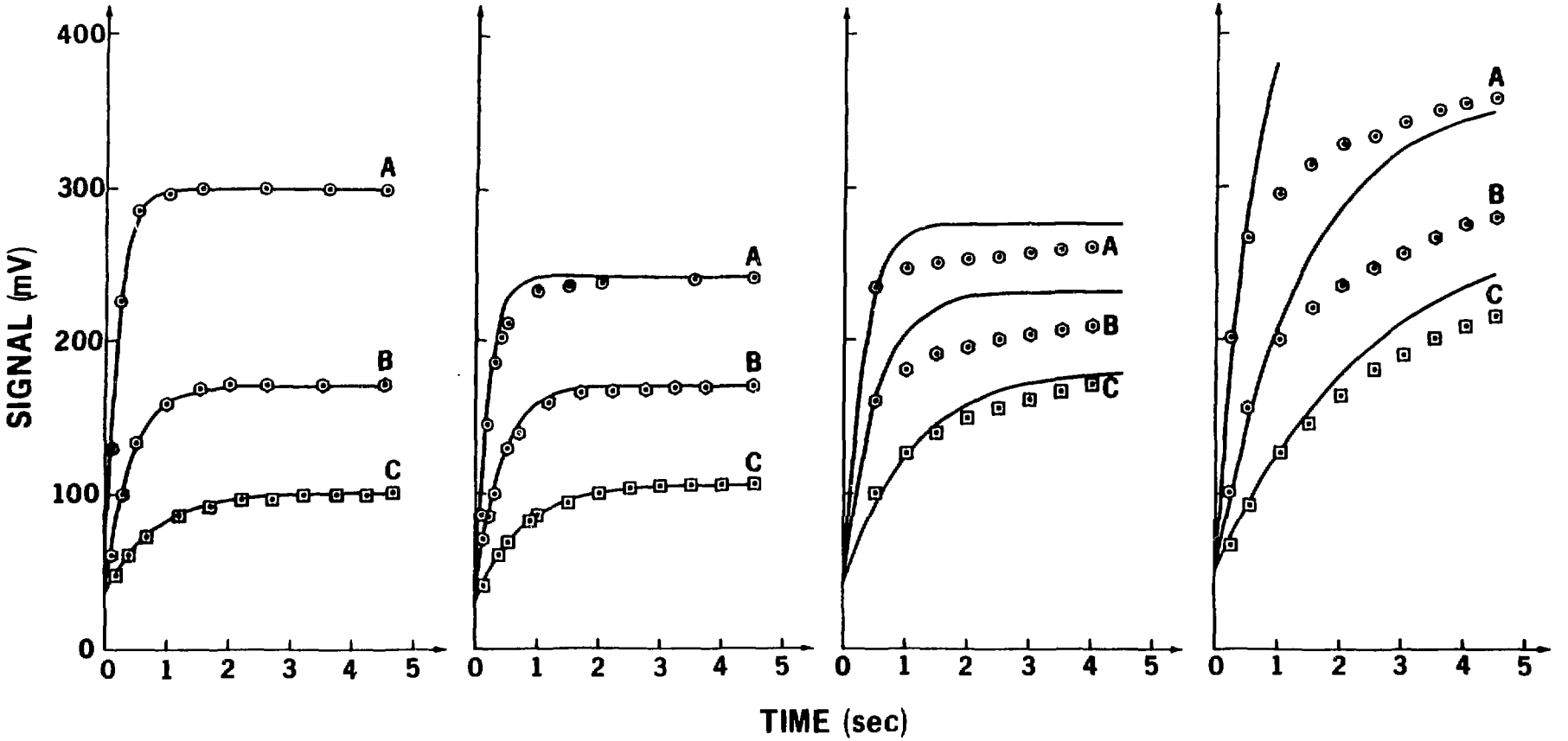

Figure 41

Transient response of four Ge:Be detectors to increased illumination
From left: 1) fully illuminated contact 2) 1x1 mm^2 3) 1x3 mm^2 4) 3x3 mm^2
Solid lines represent a calculated response with two time constants.
Note the additional slow component appearing in the large area detectors.

The appearance of the additional slow component for the large area side-illuminated device makes it difficult to obtain a good value of the time constant for the slow component which is common to all detectors. The values for τ and current density J are given in Table 7 for the thin detector, the 1x1 mm^2, and the 1x3 mm^2. The slightly longer time constant for increasing contact area may be due to the additional slow component since a two time constant model was assumed in all the fits and is clearly not correct even for the 1x3 mm^2 cases. The conclusion of the effect on τ of current density then is that τ is either independent or very weakly dependent on current density, since J varies by a factor of 15 while τ varies by less than a factor of two in all cases for a constant temperature.

TABLE 7

Time Constant as a Function of Current Density

Detector Area (mm^2)	J (arb. units)	τ * (seconds)		
		T = 3.0 K	2.73 K	2.60 K
0.2	15	0.2	0.4	0.8
1.0	3	0.2	0.4	0.9
3.0	1	0.3	0.5	1.1

* all values ± 0.1 seconds

4.4.4 Material Parameters

Although all of the Ge:Be and Ge:Zn photoconductors tested under low background conditions (as well as all Ge:Ga detectors, which have also been studied extensively) display "slow" transient behavior, the relative amplitudes and response times of the slow components vary greatly in different materials. Because contact fabrication was the same for all the detectors, this indicates that the bulk material doping, whether in the bulk or in the near-contact region, is a critical parameter in transient behavior.

The growth conditions and results of crystal characterization for a large number of detectors are summarized in Tables 8 and 9. The indication of the presence of the slow time constant behavior of interest in this study was based on the following criteria:

1. Was a slow component observed which was comparable in amplitude at some point to the fast component?

2. Did the time constant of the slow component decrease and the amplitude increase with increasing temperature?

The following trends can be observed from a survey of the detectors which were studied:

1. The large slow component (>10% of the total signal) was only observed in materials grown under a gas ambient. None of the vacuum-grown Be crystals showed this type of behavior.

2. The large slow component was present in closely compensated samples and increased in amplitude with increasing compensation. Increasing compensation along the length of the crystal also results in higher resistivity material for comparably doped material at a given temperature. Samples taken from farther from the seed end of a crystal

TABLE 8

Ge:Zn Detector Summary

Crystal No.	714				715				
Growth Conditions	CZ growth from SiO_2 crucible under H_2				CZ growth from carbon susceptor under N_2				
Detector Material	-4.8	-10.5	-10.5	-10.5	-3.5	-6.7	-9.6	-10.5	-10.5
	As Grown	Annealed 126 min. 660°C	Annealed 156 min. 660°C	Annealed 180 min. 660°C	As Grown	As Grown	As Grown	As Grown	Annealed 5 hrs. 660°C
Zn Conc. (cm^{-3})	9×10^{14}	10^{15}	10^{15}	10^{15}	2×10^{14}	2×10^{14}	1.5×10^{14}	1.5×10^{14}	1.5×10^{14}
Shallow Level Charact.	N_A-N_D $=10^{13}$	N_A-N_D $=2\times10^{12}$	N_A-N_D $=10^{12}$	N_D-N_A $=2\times10^{12}$	N_A-N_D $=3\times10^{12}$	-	N_A-N_D $=3\times10^{11}$	$N_A=N_D$	-
	$N_D=4\times10^{12}$	$N_D=6\times10^{12}$	$N_D=6\times10^{12}$	$N_D=6\times10^{12}$	$N_D=8\times10^{11}$	-	-	-	-
Slow Transient Observed	NO	YES T>4.2K	YES T>4.2K	NO	NO	YES T>4.2K	YES T>4.2K	YES T>4.2K	YES T>4.2K
Ratio: Slow/Fast	-	>1	>1	-	-	<1	>1	>1	>1

TABLE 9

Ge:Be Detector Summary

Crystal No.	719					728	
Growth Conditions	CZ growth from carbon susceptor under H_2					CZ growth from carbon susceptor under vacuum	
Detector Material	-5.6	-5.6	-5.0	-7.0	-11.6	-4.6	-4.6
	As Grown	Annealed 90 min. 600°C	Annealed 5 hrs. 660°C	Annealed 1 hr 500°C after implant	As Grown	As Grown	Annealed 2 hrs. 660°C
Be Conc. (cm^{-3})	1.5×10^{14}	1.5×10^{14}	1.5×10^{14}	1.5×10^{14}	1.0×10^{14}	5×10^{14}	5×10^{14}
Shallow Level Charact. (cm^{-3})	N_A-N_D $=2\times10^{12}$	N_A-N_D $=6\times10^{11}$	N_A-N_D $=6\times10^{12}$	N_A-N_D $=2\times10^{12}$	N_A-N_D $=2\times10^{12}$	N_A-N_D $=10^{13}$	N_D-N_A $=10^{12}$
Slow Transient Observed	YES T=2-3K	YES T=2-3K	YES T=2-3K	YES T=2-3K	YES T=2-3K	NO	NO
Ratio: Slow/Fast	>1	>1	>1	>1	>1	-	-

also generally have a higher dislocation density since the dislocations multiply during crystal growth.

3. In the Ge:Zn crystal, the slow component behavior disappeared when the shallow acceptors became overcompensated (i.e., change from $N_A>N_D$ to $N_A<N_D$).

4. Extensive annealing of both Ge:Zn and Ge:Be which did not cause a change in shallow level compensation did not greatly affect the transient behavior.

In order to determine if the slow transient behavior was also present, though in a different way, in the vacuum grown crystals, a comparison of DC and AC (20 Hz) data as a function of temperature is compiled in Figure 42 for a variety of crystals. One sees that all display evidence of slow components, but in the vacuum grown case, the amplitude of the component is much smaller.

It is apparent from the collection of data that the materials dependences of the phenomena are relatively complicated, since the crystals do not vary greatly in terms of either primary or shallow level doping and there are many parameters combinations to be considered. Deep level transient spectroscopy studies were done along the length of Ge:Zn crystal 714 to determine if the appearance of any deep levels would be coincident with the appearance of the large slow transient response. No deep levels were detectable at any point, however, down to a limiting concentration of $\approx 10^{10}$ cm^{-3}, equivalent to 1% of the shallow level doping.

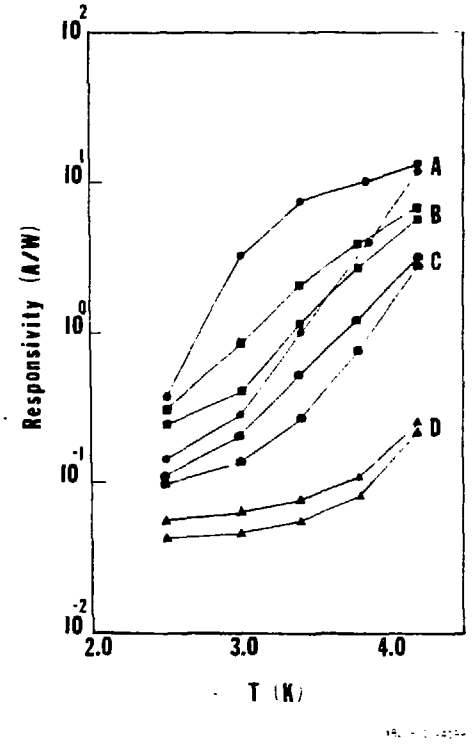

Figure 42
DC and AC (20 Hz) responsivity as a function of temperature for H_2 grown and vacuum grown crystals
A) H_2 grown B–D) vacuum grown

4.4.5 Lifetime Measurements

Measurements of free carrier lifetime as a function of photon flux were made to determine if the slow transient response was caused by an increase in lifetime with increased illumination. This was tested in the following way. The transient response of the detector to a step function increase in photon flux was measured to determine the amplitude and speed of the response. Then, while maintaining the higher flux level as the new background, an additional signal Δp of the same size as the previous signal was imposed. In this way it was possible to determine the

responsivity at each level of background flux. The responsivity is a function only of lifetime for a given detector at fixed electric field and temperature. Results of the experiment are summarized in Figure 43.

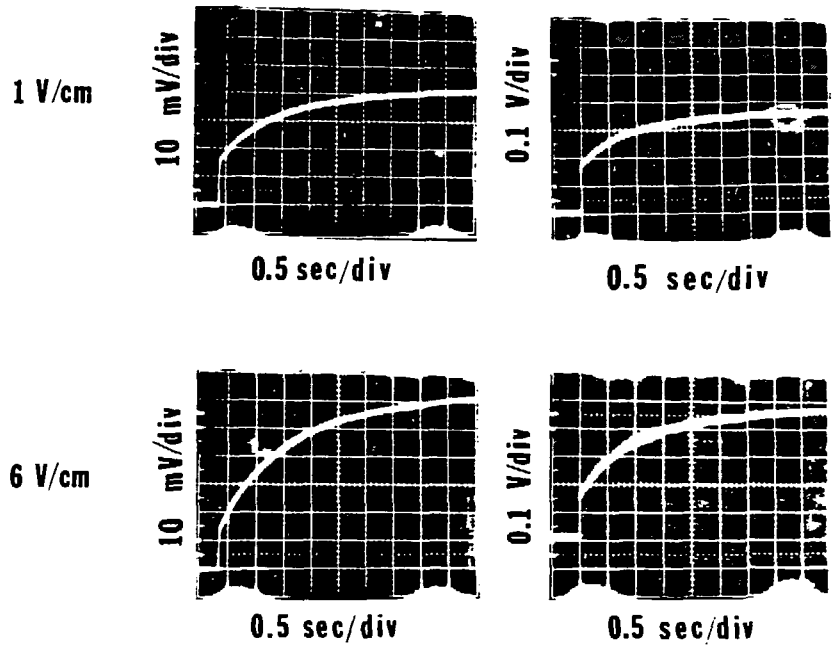

$T_{background}$	77 K	300 K
	1.5×10^8 p/s	8.9×10^8 p/s
T_{signal}	300 K	497 K
	8.9×10^8 p/s	1.6×10^9 p/s
Signal (Δ)	7.4×10^8 p/s	7.1×10^8 p/s
Responsivity (A/W)		
1 V/cm	0.53	0.44
6 V/cm	7.9	5.8
τ (sec)		
1 V/cm	1.6	1.1
6 V/cm	1.7	1.2

Figure 43

One sees that the photoconductive gain did not increase at the higher flux level, but in fact decreased by ~20%. This could be a real effect but is more likely due to the uncertainty (±20%) in the calculation of the photon flux which requires mixing the effects of the blackbody source and the room temperature emission from the window. If the slow component were due to an increase in lifetime, however, one would expect an increase of a factor of 2-3 in responsivity since this is the increase in responsivity due to the slow component in the transient, and this is clearly not observed. This result also confirms earlier results showing that the time constant τ is not directly proportional to the background hole concentration. The decrease that was noted in τ (~ a factor of 1.5) may reflect a weak dependence on background flux or the heating of the detector that occurs when the field of view of the dewar is filled with the hot external blackbody. This heating is known to occur because the reading of the temperature sensing resistor indicates a temperature rise when the radiation from the hot blackbody enters the dewar.

4.5 Discussion and Evaluation of Experimental Results

The unique features of the behavior which has been observed in these detectors include a temperature-dependent transient with time constants on the order of seconds, which is not dependent on electric field or material resistivity. There are material dependences, and the phenomena is observed only in closely compensated samples. We will survey the data in order to compare it to our present understanding of transient behavior and to see what features must be included in the development of new models.

A survey of time constants associated with the measured transient behavior, free carrier lifetime, and dielectric relaxation time for the Ge:Zn and Ge:Be detectors is presented in Table 10. Free carrier lifetimes, τ_l, were determined from measured dc responsivity values, while the dielectric relaxation time constant, τ_ρ, can be determined directly from a measurement of detector resistance and geometry, i.e.,

$$\tau_l = R e \mu E/(h\nu L) \qquad (4.10)$$

and

$$\tau_\rho = \rho\varepsilon\varepsilon_0. \qquad (4.11)$$

TABLE 10

Survey of Detector Time Constants

	$\tau_{lifetime}$ (sec)	τ_ρ (sec)	$\tau_{slow\ component}$ (sec)
Ge:Be			
T = 2.7 K E = 1 V/cm	3×10^{-9}	2.8×10^{-2}	1.6
T = 2.7 K E = 6 V/cm	8×10^{-9}	1.4×10^{-2}	1.7
Ge:Zn			
T = 5.6 K E = 0.5 V/cm	2.5×10^{-8}	3.0×10^{-3}	1.2
T = 7.0 K E = 0.5 V/cm	1.5×10^{-8}	5.5×10^{-5}	0.9

The comparison between these time constants shows that the observed response is orders of magnitude longer than both the dielectric time constant and the lifetime. This conclusion is also supported by a number

of experiments. The difference in the effect of increased background flux versus increased temperature (Figure 36) showed that what is important is not the resistivity or the concentration of free holes, but rather the lattice temperature of the device. Dielectric relaxation, in contrast, is resistivity dependent. Also, dielectric relaxation theory predicts that the fast component should saturate with increasing bias once sweep-out effects begin. This is also not the case here, as Figure 39 has shown. The first conclusion therefore is that the observed response cannot be attributed to a lifetime controlled or dielectric relaxation controlled process.

The correlation between the appearance of the slow component and close compensation of many of the samples raises the question of whether the lifetime increase due to close compensation discussed in Chapter 3 may be responsible for the slow component. The strong temperature dependence of the amplitude of the slow component is explained by the free carrier lifetime increase as a function of temperature that has been observed in the Ge:Be and Ge:Zn detectors. Since the lifetime is known to be increasing rapidly in the temperature ranges where the transient is observed, one could posit that the τ of the response is proportional to the free carrier lifetime which is determined by the distribution of trapped charge between the shallow and semideep levels. It is important to distinguish between temperature dependence and flux dependence of the lifetime. Results showing that the lifetime is not increasing with increased flux indicate that the transient itself is not a result of increasing lifetime. The total amplitude of the signal, however, is explained by the close compensation of the material.

The analysis of annealed samples for several of the detectors (719-5.6, 719-11.6, 715-10.4) was performed to determine if the outdiffusion of H_2 or any other trapped gases affected the transient response. This question arose in view of the fact that the relative amplitude of the slow component was largest in crystals grown under a H_2 or N_2 atmosphere. In all cases where the annealing behavior did not greatly affect the shallow level compensation, the transient behavior was unchanged after annealing. One concludes that the H and H-related centers which have previously been discussed in Chapter 3 and shown to anneal away at these temperatures do not play a major role in the transient behavior.

The temperature dependence of the time constant of the transient response can be analyzed from several perspectives. The "activation energy" associated with the time constant (~2.5 meV for Ge:Be, ~3.2 meV for Ge:Zn) indicates an effect involving shallow levels or contact behavior rather than the primary dopant levels or the presence of deep levels. Although energies of <5 meV do not correspond to any known elemental dopants, one must remember that an illuminated photoconductor is not simply in thermal equilibrium and that the Fermi level is actually given by a quasi-Fermi level which, at low temperatures, is determined entirely by the photon flux.

Figure 44 shows the position of the quasi-Fermi level and the thermal equilibrium Fermi level in the dark as a function of temperature for the parameters listed. One sees that the quasi-Fermi level is less than the ionization energy of the shallow levels for the temperatures and photon fluxes at which the photoconductors operate. The quasi-Fermi level also increases with increasing temperature for a given flux, which may explain

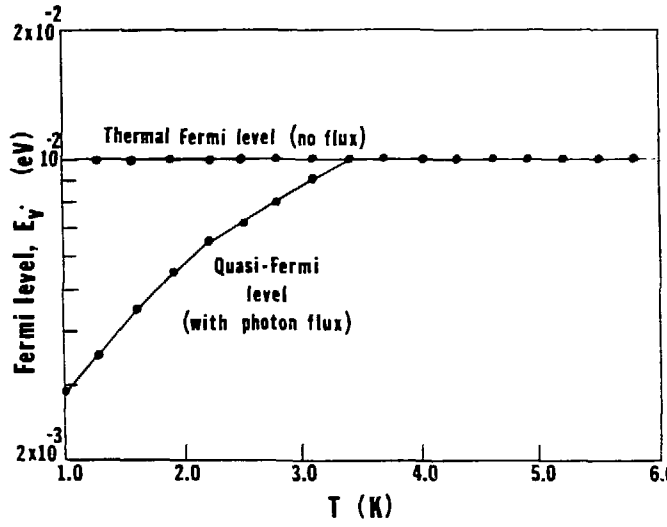

Figure 44
Calculated Fermi levels for illuminated and nonilluminated material with: $N_{Be} = 5 \times 10^{14}$ cm^{-3}, $N_A = 10^{12}$ cm^{-3}, $N_D = 5 \times 10^{11}$ cm^{-3}, $\sigma = 1 \times 10^{-12}$ cm^2, $Q = 5 \times 10^{10}$ p/s.

why a higher "barrier" is measured for Ge:Zn than for Ge:Be. More importantly, the only place in the device where barriers might exist which are related to the quasi-Fermi level is in the near contact region (See Chapter 5). This is the first experimental evidence pointing to near-contact behavior as the source of the slow transient response.

Other experiments were designed to isolate the transient response as a near-contact or bulk phenomena. Refering again to the current equation, neglecting diffusion terms,

$$J = pe\mu E + \epsilon dE(x,,,/dt \qquad (4.12)$$

or $$dJ/dt = e\mu Edp/dt + e\mu pdE/dt + \epsilon d^2E/dt^2 \qquad (4.13)$$

Current transients, therefore, must arise due to transient changes in

either electric field or hole concentration. Since the hole concentration in the bulk of the sample is given by $p=\mathring{p}\tau$, changes in free hole concentration in the bulk will only occur if there is a change in free carrier lifetime, neglecting sweep-out effects. The experimental results showing that the free carrier lifetime is not increasing with increasing illumination (Figure 43) indicates that the dp/dt term can be neglected to first order, and that the current transient must arise from slow transients in the electric field. Because the profile of the electric field in a photoconductor is determined mainly by trapped space charge near the contact, this is a second argument in support of the idea that the slow transient is not a bulk effect.

Finally, comparing the experimental observations in Ge:Be and Ge:Zn to Lampert and Rose's theory for the transient behavior of ohmic contacts, one finds that, although the theory cannot account for all the experimental results, it does predict certain features. Recalling Equation 4.9:

$$\tau_c = \frac{A}{F}\left(\frac{\epsilon k T N_T}{e^2}\right)^{1/2} \qquad (4.9)$$

one sees that τ_c is temperature-dependent ($T^{0.5}$ plus an implicit temperature-dependence of N_T) but does not depend on free hole concentration or electric field. Also, the model predicts a symmetric rise and decay response, which has been observed in most of the Ge:Be and Ge:Zn devices under constant voltage. Finally, material variations would be expected due to variation in N_T, the trapped space charge near the contact. On the other hand, the time constant calculated using Equation 4.9 is several orders of magnitude shorter than the observed transient, and it has been shown experimentally that τ_c is not directly

proportional to contact area (i.e., current density).

The Lampert-Rose model is purely phenomenological in its treatment of how space charge is "rearranged" at the contact barrier, dealing only with optical generation but not recombination. In addition, the assumption of constant trapped charge, N_T, is not valid in a cold extrinsic photoconductor. The prediction, however, that even nominally "ideal" contacts may lead to transient behavior which is slower than any bulk effect is important. In the next and final Chapter, we will review the theory of the ohmic contact and present some recent modeling attempts to begin to numerically determine the transient behavior associated with electric field changes in the near contact region.

Chapter 5 Ohmic Contacts to Far Infrared Photoconductors

5.1 Theory

An ohmic contact is generally defined as a metal-semiconductor contact that has a negligible resistance compared to the resistance of the bulk material. According to Sze, an ohmic contact is one that "should not significantly perturb device performance...and can supply the required current with a voltage drop that is sufficiently small compared with the drop across the active region of the device" (51). One method of achieving this is to form, either through diffusion, implantation, or alloy regrowth, a heavily doped surface layer in the semiconductor. Carriers can then tunnel through the metal-semiconductor barrier and the ability of the contact to supply carriers will be independent of the barrier height ϕ_B.

Most of the data on ohmic contacts are for room temperature contact to Si and III-V and II-VI devices, where either a low barrier height or a tunneling contact will lead to ohmic characteristics. For cooled IR photoconductors, however, the available thermal energy is very small (0.36 meV at 4.2 K), so the contact must be a tunneling contact. The impurity concentration in the heavily doped layer must be high enough to exceed the metal-semiconductor transition, i.e., the Fermi level must lie within the valence band at all temperatures for ohmic contact to a p-type device. This will lead to a reservoir of free holes in the semiconductor and the carriers can move through the metal-semiconductor barrier at any temperature.

The free carriers in the contact region do not diffuse throughout the semiconductor bulk because there is an additional diffusion barrier

E_V-E_F which exists due to the space charge generated when free holes diffuse into the bulk near the contact and are trapped by ionized acceptors. This leads to a region of trapped space charge in the near-contact region. The barrier is shown in Figure 45, which displays the space charge, electric field, potential, and the energy band diagram for the near-contact region with and without an applied field. A linear distribution of ρ has been assumed only for schematic simplicity. This figure shows that there is a point where the potential energy goes through a maximum for holes. This occurs at the point where the electric field is equal to zero, a point of pure diffusion current. The small barrier for free holes from the implanted region to the bulk is usually neglected in discussions of ohmic contacts because in most cases it is small compared to the thermal energy at room temperature. It is not immediately clear, however, that this can be neglected in a device operated at 4 K. When one speaks, therefore, about the contact barrier in an extrinsic Ge photoconductor, one is usually not referring to the metal-semiconductor barrier, which is assumed to be negligible due to the tunneling contact, but rather to the small diffusion barrier in the material itself.

5.2 Contact Modeling

Very little attention has been given to low temperature ohmic contacts, both because of their limited use and the mathematical complexity of including contact effects in the transport equations. Recently, however, some attempts have been made to solve the differential equations describing steady state carrier transport, including the boundary condition for an ideal ohmic contact (52). The equations

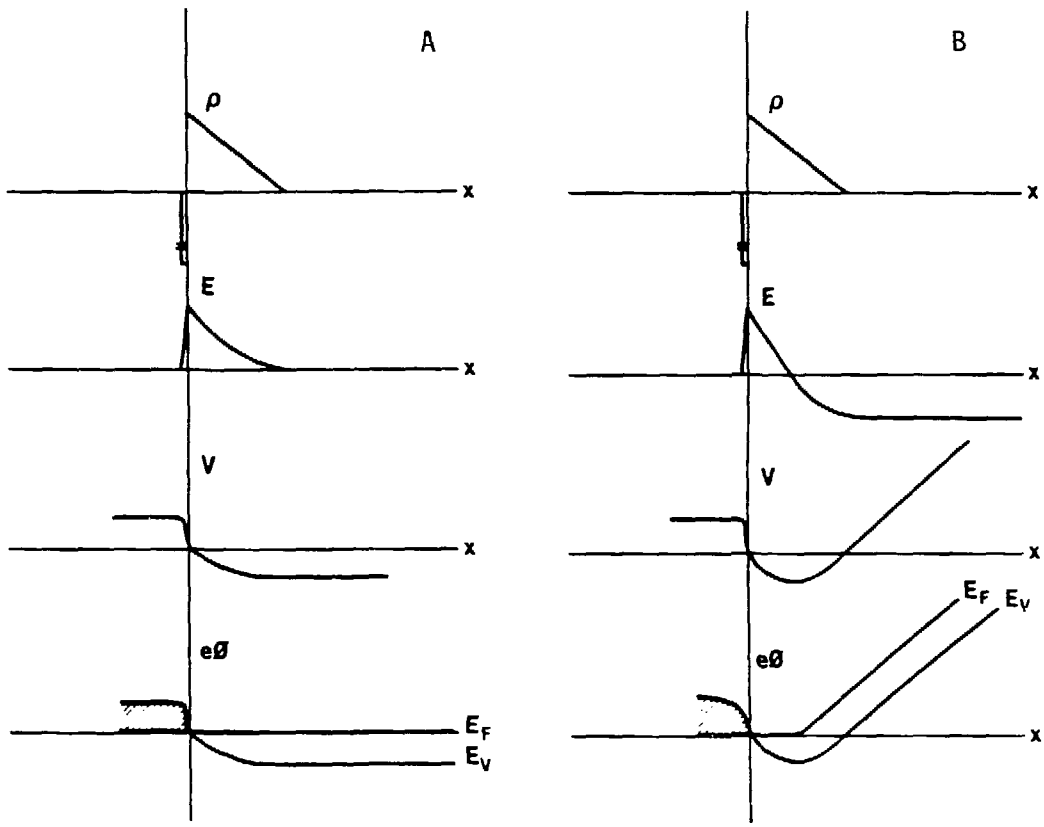

Figure 45

Space charge, electric field, potential, and band diagram as a function of distance in the near-contact region A) without applied external bias and B) with applied external bias.

governing the physics of the near-contact region will be reviewed and a summary of the steady state solution will be given. Then, the extension of the model to time-dependent behavior will be described.

5.2.1 Physics of the Near-Contact Region

The physics of the near-contact region is dominated by the space charge which exists due to the diffusion of free holes from the contact into the bulk material. This occurs because of the large concentration gradient between the implanted layer ($p \sim 10^{20}$ cm^{-3}) and the bulk material ($p < 10^{2}$ cm^{-3} under low background operating conditions). Like the diffusion of electrons and holes across a p-n junction, this process is stopped by the build-up of a space charge region. At low temperatures, the free holes will be trapped (i.e., recombine into the ground state) on the ionized acceptors which are present due to compensation, leading to the build-up of a positive space charge.

Using the same formulation as Reference 52, the time-dependent partial differential equations for carrier transport throuhg a one-dimensional sample are given by:

$$\partial a^*/\partial t = \gamma(a - a^*) + p[k(a - a^*) - ra^*] \qquad (5.1)$$

$$\partial p/\partial t + v_d \partial p/\partial x = \partial a^*/\partial t \quad (d - a^* + p)(pe/\varepsilon)(dv_d/dE) \qquad (5.2)$$

$$\partial E/\partial t = (J_{ext} - pev_d)/\varepsilon \qquad (5.3)$$

where
- a^* = ionized acceptor concentration
- a = neutral acceptor concentraion
- p = free hole concentation
- k = impact ionization coefficent
- E = electric field
- ε = dielectric constant
- v_d = hole drift velocity
- r = recombination coefficient

Equation 5.1 is simply a rate equation, indicating the balance between generation and recombination processes. Equation 5.2 is a one-dimensional form of the continuity equation

$$dp/dt = G - U - (1/e)\,\nabla \cdot J \qquad (5.4)$$

which says that the change in free hole concentration with time must be given by the balance of generation (G) and recombination (U) and the gradient of the current. Finally, Equation 5.3 states that the external current will be the sum of the current due to the motion of free holes and the displacement current in the device.

To include the contact region in the solution of these equations, one must select a boundary condition to approximate the physical behavior near the contact. In the work of Westervelt and Teitsworth (52), this was done by setting E=0 at the contact and allowing $p \to \infty$ at x=0 to keep the current finite. To first order, this appears to be a very realistic modeling assumption, since E must go to zero at the boundary of the device and $p_c >> p_{bulk}$ at the contact. In addition, modeling of the free hole distribution in an insulator under trap free conditions results in a free hole distribution of $p \sim 1/x$ near the contact. This model, therefore, gives the correct asymptotic behavior for the approach to the contact where p is much greater than the trap concentation.

In the steady state, all time derivatives go to zero and the problem becomes that of integrating a single differential equation. Steady state solution for two different currents are given in Figure 46 for the parameters given. Note the changes in ionized acceptor distribution and field distribution which must occur to allow for this change in the steady state operation. It is also important to note that this modeling was done under a constant current assumption, i.e., J_{ext} = constant,

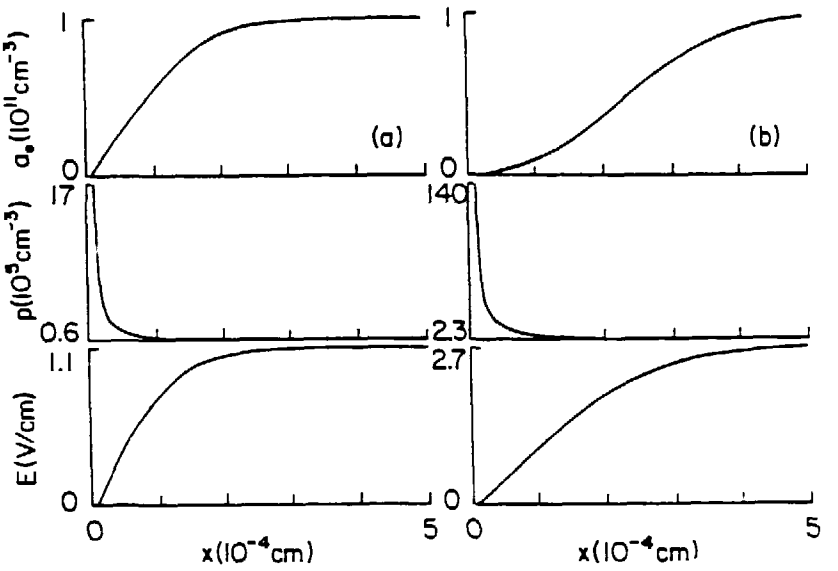

Quantity	Value
acceptor concentration	$a = 1 \times 10^{14}\ \mathrm{cm}^{-3}$
donor concentration	$d = 1 \times 10^{11}\ \mathrm{cm}^{-3}$
hole effective mass	$m^* = 0.35\ m_0$
dielectric constant	$\epsilon = 16$
temperature	$T = 4.2\ \mathrm{K}$
generation coefficient	$\gamma = 1 \times 10^{-4}\ \mathrm{sec}^{-1}$
hole mobility	$\mu = 1 \times 10^{6}\ \mathrm{cm}^2/\mathrm{V\ sec}$
saturation velocity	$v_s = 1 \times 10^{7}\ \mathrm{cm/sec}$
hot carrier spreading coefficient	$\eta = 1$
recombination coefficient	$r_0 = 3 \times 10^{-6}\ \mathrm{cm}^3/\mathrm{sec}$
impact ionization coefficient	$\kappa_0 = 6 \times 10^{-6}\ \mathrm{cm}^3/\mathrm{sec}$
impurity ionization energy	$B = 10\ \mathrm{meV}$

Figure 46
Steady state solutions for $J=10^{-8}$ A/cm^2 and $J=10^{-7}$ A/cm^2 for the parameters listed (Ref. 52)

for mathematical simplicity.

As a first step toward the transient solution, Westervelt and Teitsworth constructed a simplified two-region model (near-contact and bulk) which is valid only on a long time constant scale. Results are presented in Reference 52 and will not be reviewed here, but the important conclusion is that they predicted slow transient responses on the order of > 1 second. The status of the modeling at this point leaves unanswered any questions concerning the relative magnitude of the predicted slow response or the effects of bias, temperature, background flux, etc., and a complete solution of the time dependent equations is required. A physical phenomena in the device is identified, however, which is occuring on a time scale much longer than the free carrier lifetime or the dielectric relaxation involving free holes.

5.2.2 Time Dependent Solutions for the Near-Contact Region

In collaboration with Westervelt and Teitsworth, the model has now been extended to include numerical solutions for the full time and space dependent partial differential equations. This was done by solving for the initial steady state solution under a fixed level of illumination using a numerical integration technique called the Gear method (55). This is a variable step size technique for so-called "stiff" equations, equations with transient terms that vary greatly in the time domain. The steady state solutions, $E(x,0)$, $a^*(x,0)$ and $p(x,0)$, were then used as the initial conditions to determine the transient response to a step increment in illumination.

The time derivative in a^* (Equation 5.1) was calculated using a first order Euler technique. Equation 5.2 was reduced to an ordinary different

equation by assuming that $\partial p/\partial t << v_d \partial p/\partial x$, equivalent to assuming that the transit time of a free hole in the near contact region is small compared to the lifetime. Since our photoconductors have photoconductive gains of 0.1 to ~1 carriers/photon this seems to be a good assumption. Solutions for E(x) and p(x) at the new time t + Δt can then be determined by integrating the following two coupled differential equations in x:

$$\partial p/\partial x = +(1/v_d)\partial a^*/\partial t - (pe/\varepsilon v_d)(d-a^*+p)dv_d/dE \quad (5.4)$$

$$\partial E/\partial x = e/\varepsilon\ (d+p-a^*) \quad (5.5)$$

The Gear method was also used to perform this integration.

A representative series of solutions for E(x) and a*(x) as a function of time are given in Figure 47. One sees that the new steady state solution is not achieved until ~5 seconds after the change of generation rate. In the first surveys of this model, time constants ranging from 3 to 10 seconds have been required before total damping of the oscillations to the final steady state was achieved. The oscillatory nature of the solutions is a new feature which was not predicted by the earlier two stage model.

5.3 Analysis of Current Modeling Status and Suggestions for Future Work

Although significant progress has been made in identifying a slow transient process in nominally "ideal" photoconductors and in solving the time dependent solutions for a realistic case which includes space charge and contact effects, there is still a large amount of work to be done before the model can be compared to experimental data. The voltage output from the device is the integral under the electric field curve. To determine the voltage (or current) transient one must integrate the electric field expression over a finite distance comparable to the

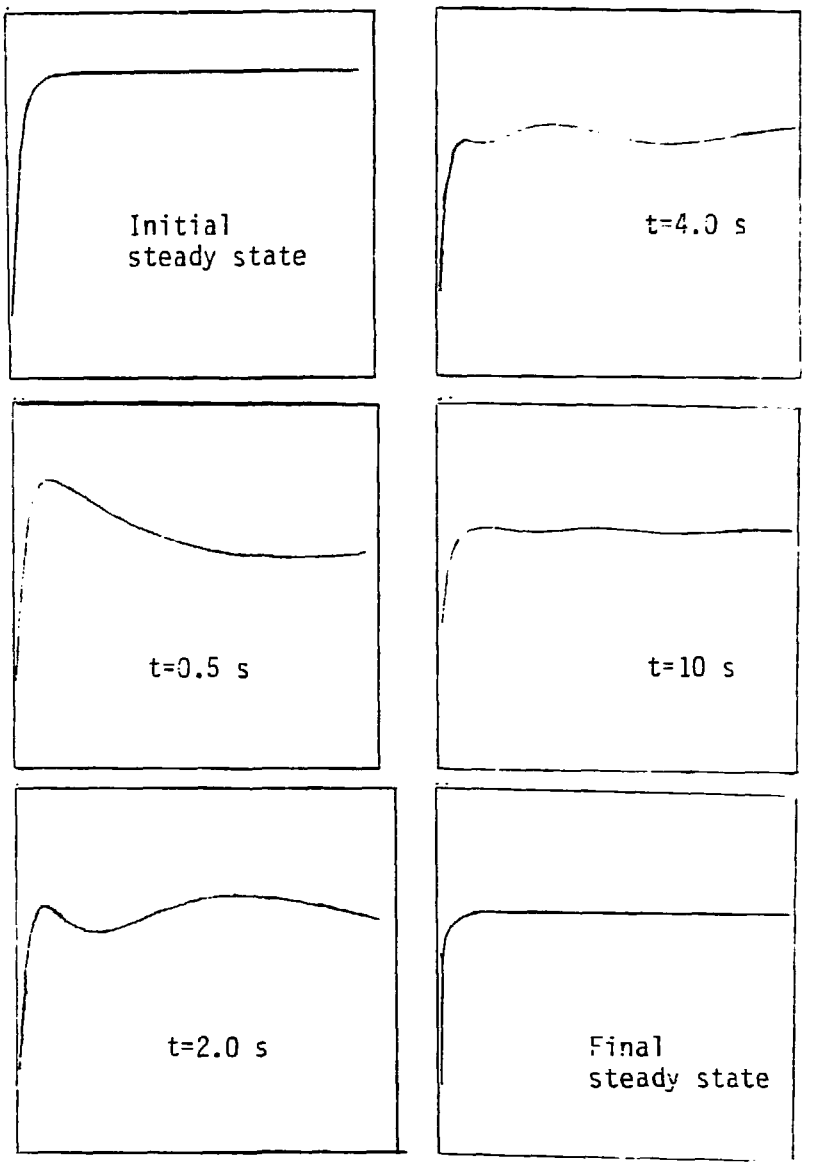

Figure 47

Calculated transient response for parameters of Figure 46 to an increase of current such that $J_{final} = 1.3\ J_{initial}$ ($J_{initial}=10^{-7}$ A/cm^2).

All data plotted as Electric field (0 to 2.0 V/cm) versus distance from contact (0 to 5×10^{-3} cm).

intercontact distance of the device. This will require including the effect of the other contact and adding the appropriate boundary condition.

A second issue concerns the energy barrier for the injection of holes which was discussed in the previous sections. That barrier is not included in this model because the integration begins at the point where E=0, i.e., no barrier to the injection of holes exists in the Westervelt model. The adjustment of the barrier height is assumed to be instantaneous and only the rearrangement of space charge beyond that point is considered. This is in contrast to the Rose model which concerns itself with the readjustment of that barrier height, but in a purely phenomenological way. To include the contact barrier in the model, the range of integration must be extended back into the region where the electric field is negative. This changes the E=0 boundary condition and replaces it with a condition that the current at the point E=0 is a pure diffusion current and directly proportional to the concentration gradient of free holes.

Both of these issues need to be addressed in order to explain the amplitude of the transient responses which are observed and to begin to addresss the materials dependence of the responses. A second model, which includes a second level to simulate a multi-level system such as Ge:Be or Ge:Zn is also in progress. The addition of a second level would allow one to explore the dynamics of the transient distribution of space charge both energetically among the various levels as well as spatially within the device.

6.0 Summary and Conclusions

The temperature-dependent and transient behavior of Ge:Be and Ge:Zn photoconductors have been studied experimentally and attempts have been made to understand these behaviors in terms of the most recent model for low background extrinsic photoconductors. The following points summarize the main conclusions:

- Ge:Be material can be successfully grown and detectors have been sufficiently characterized to allow for the use of these devices in future astronomy and astrophysics applications in space. Ge:Be detectors provide improved performance in the 30-50 μm wavelength range.
- The responsivity of Ge:Be and Ge:Zn photoconductors is strongly temperature-dependent in closely compensated material.
- The experimental data for the responsivity as a function of temperature in Ge:Be detectors can be fit using the model of Alexander et.al. by taking into account the temperature dependence of the recombination cross section.
- Novel shallow acceptors, A(Be,H) and A(Zn,H), exist in doped crystals grown under a H_2 atmosphere. Their concentration can be reduced with thermal annealing and can be controlled in order to obtain very closely compensated material.
- The large lifetime increase with temperature in closely compensated Ge:Be has been observed using photo-Hall effect.
- Transient behavior has been observed in both Ge:Be and Ge:Zn with time constants on the order of seconds. It has been established that this cannot be explained by carrier sweep-out and/or dielectric relaxation.

- The transient behavior has been characterized as a function of temperature, bias, contact area, photoconductive gain, and material parameters.
- Time-dependent solutions of the transport equations, including space charge in the near contact region, have been obtained for the first time. The results indicate that transient phenomena with time constants on the order of seconds occur due to changes in the electric field and ionized acceptor concentrations in the near contact region.

The experimental charcterization of the temperature dependence of the responsivity in the Ge:Be detectors is important for their use in astronomy applications and will affect the selection of material for future satellite-based missions. Work still remains to be done in achieving, in a controlled fashion, the very high responsivities predicted by theory. However, responsivities of ~ 1.0 carrier/photon have been achieved in as-grown material.

The transient phenomena are still far from being fully understood. Many factors have been identified which point toward a near-contact controlled response which is several orders of magnitude slower than predicted by other theories. Theoretical evidence for this has come from first attempts to solve time-dependent equations for a realistic model which includes space charge in the near contact region.

The most important question remaining is why the amplitude of the slow component can be so large a part of the signal in certain Ge:Be and Ge:Zn materials. The observation and systematic study of this benavior, however, has been helpful in moving the analysis of transient phenomena toward a more integrated effort involving both experiment and theory.

Demands for improved performance and understanding of extrinsic photoconductors will continue to grow as the application of these devices extends to lower backgrounds in the quest for greater sensitivity and observing power. When the pioneers in the field gathered in Atlantic City in 1954, they probably did not imagine that thirty years later we would be developing Ge:Be photoconductors to be sent into space on an orbiting telescope at 2 K to look for distant galaxies and new stars. The "fascinating diversions of itinerant electrons and holes" continue to find fascinating applications.

References

1. Breckenridge R G and Russel B R, Photoconductivity Conference, (New York: John Wiley and Sons, Inc.) vii, 1956.

2. Burnham R, "IRAS and the Infrared Universe," Astronomy, 12, 6, 1984.

3. Mather J C, J. Optical Engineering 21, 769 (1982).

4. Infrared Space Observatory, Report on Phase A Study, European Space Agency Sci (82) 6, (1982).

5. Gillett F C and Werner M W, "SIRTF - The Next Step," NASA Technical Memo. 86663, 1984.

6. McCreight C R, Proceedings of the IAU Coll. No. 79, Garching, April9-12, 1984.

7. McCreight C R, et. al., Proc. SPIE, 28th Int. Tech. Symp., 1984.

8. Brovdy R M and Mazurczyck V J "(HgCd)Te Photoconductive Detectors," in: Semiconductors and Semimetals, Willardson R K and Beer A C, eds. (New York: Academic Press) 18, 157-198, 1981.

9. Reine M B, Sood A K, and Tredwell T J, "Photovoltaic Infrared Detectors," in: Semiconductors and Semimetals, Willardson R K and Beer A C, eds. (New York: Academic Press) 18, 201-305, 1981.

10. Stillman G E, Wolfe C M and Dimmock J O, "Far-Infrared Photoconductivity in High Purity GaAs," in: Semiconductors and Semimetals, Willardson R K and Beer A C, eds. (New York: Academic Press) 12, 291, 1977.

11. Bratt P R, "Impurity Germanium and Silicon Infrared Detectors," in: Semiconductors and Semimetals, Willardson R K and Beer A C, eds. (New York: Academic Press) 12, , 1977.

12. Bube R H, Photoconductivity in Solids (New York: John Wiley and Sons, Inc.), 1960.

13. Rittner E S, "Electron Processs in Photoconductors," in: Photoconductivity Conference, Breckenridge R G and Russel B R eds. (New York: John Wiley and Sons, Inc.), 215-268, 1956.

14. Rose A, RCA Review 12, 362 (1951).

15. Haegel N M, Hueschen M R, and Haller E E, Infrared Physics 25, 273 (1985).

16. Keyes R J and Quist T M, "Low-level Coherent and Incoherent Detection in the Infrared," in: Semiconductors and Semimetals, Willardson R K and Beer A C eds. (New York: Academic Press) 5, 322-328, 1970.

17. Haegel N M, Haller E E, and Luke P N, Intl. J. Infrared and Millimeter Waves 4, 945 (1983).

18. Haegel N M, "Performance and Materials Aspwxra od Ge:Be and Ge:Ga Photoconductors for Far Infrared Detection," MS Thesis, University of California, Berkeley, 1983. LBL-16694.

19. Cross J W, Ho L T, Ramdas A K, Sauer R and Haller E E, Phys. Rev. B 28, 6953 (1983)

20. Shenker H, Swiggard E M and Moore W J, Trans. Met. Soc. AIME 239, 347 (1967).

21. Bratt P R, Lewis N N and Long L E, Fifnal Technical Report NAS2-9385, Santa Barbara Research Corporation, 1977.

22. Brunsmann U, Egle H, Frenzl O and Dinges P, Final Report, ESTEC Contract 4458/80/NL/HP(SC), Battelle Institute, Frankfurt BDR, 1982.

23. Ramdas A K and Rodriguez S, Repts. on Progress in Physics 44, 1297, (1981).

24. Picus Gerald S, J. Phys. Chem. Solids 22, 159 (1961).

25. Levinstein H, Appl. Opt. 4, 639 (1965).

26. Goncharov L A and Kervalishvili P D, Inorgamic Materials 14, 775 (1978).

27. Hansen W L and Haller E E, Proc. Materials Research Society 1982 Annual Meeting, Symposium F, (New York: Elsevier Science) 16, 141-173, 1983.

28. Darken L S, IEEE Trans. Nucl. Sci. NS-26, 324 (1979).

29. Putley E H, The Hall Effect and Related Phenomena (London: Butterworths) 1960.

30. Haller E E, Hueschen M R, and Richards P L, Appl. Phys. Lett. 34, 495 (1979).

31. Watson D M, Ph.D. Thesis, University of California, Berkeley, 1982.

32. Low F J, SPIE 280, 56 (1981).

33. Lax M, Phys Rev. 119, 1502 (1960).

34. Abakumov V N, Perel' V I, and Yasslevich I N, Sov. Phys. Semicond. 12, 1 (1978).

35. Alexander D H, Baron R, and Stafsudd O M, IEEE Trans. Elec. Dev. ED-27, 71 (1980).

36. Geim K, Pensl G and Schultz M, Appl. Phys. A 27, 71 (1982).

37. Thomas R N, Braggins T T, Hobgood H M and Takei W J, J. Appl. Phys. 49, 2811 (1978).

38. Fritzsche H and Cuevas M, Phys. Rev. 119, 1238 (1960).

39. Haller E E, Hansen W L, and Goulding F S, Advances in Physics 30, 93 (1981).

40. Morin F J and Reiss H, Phys. Rev. 105, 384 (1957).

41. Crouch R K, Robertson J B and Gilmer Jr., T E, Phys. Rev. B 5, 3111 (1972).

42. McMurray, Jr. R E, Haegel N M, Kahn J M, and Haller E E, Solid State Comm. 53, 1137 (1985).

43. McMurray, Jr. R E, Haegel N M, Kahn J M, and Haller, E E, to be published.

44. Hansen W L, Haller E E, and Luke P N, IEEE Trans. Nuc. Sci. NS-29, (1982).

45. Kahn, J, private communication.

46. Williams R L, J. Appl. Phys. 40, 184 (1969).

47. Milton A Fenner, Appl. Phys. Lett. 16, 285 (1970).

48. Milton A Fenner and Blouke M M, Phys. Rev. B 3, 4312 (1971).

49. Lampert M A and Rose A, Phys. Rev. 113, 1236 (1959).

50. Sayre C, Arrington D, Eisenman W, and Merriam J, Opt. Eng. 16, SR-40 (1977).

51. Sze S M, Physics of Semiconductor Devices 2nd ed. (New York: John Wiley and Sons, Inc.) 304, 1981.

52. Westervelt R M and Teitsworth S W, J. Appl. Phys. 57, 5457 (1985).

53. Hall G and Watt J M, (eds), Modern Numerical Methods for Ordinary Differential Equations, (Oxford: Clarendon Press) 1976.

54. Germer T A, "The Photo Hall Effect In Beryllium Doped Germanium," Senior Thesis, 1985. LBL-19616

55. van der Pauw L J, Phillips Res. Repts. 13, 1 (1958).

Appendix 1

Thermodynamics Calculations for BeO Formation

Thermodynamics calculations based on the free energy of formation and the mass action law can given an indication of the stability of an oxide under various conditions of temperature, concentration, and environment. The following basic calculations can be used as guidelines for determining the probability of oxide precipitation.

The free energy of formation for a reaction is often modeled with the equation:

$$\Delta G = \Delta H^{o} - T\Delta S \qquad (A.1)$$

where ΔH and ΔS are considered temperature independent. For the formation of BeO:

$$2Be + O_2 \rightarrow 2BeO \qquad (A.2)$$

$\Delta H = -143{,}000$ calories and $\Delta S = 23$ calories/K.

In a germanium melt, it is necessary to consider the solution thermodynamics of a small concentration of Be in a germanium solvent. This was the approach taken by Darken (28) and applied to the stability of oxides in high-purity Ge crystal growth. The question of interest is whether Be will precipitate as an oxide in the melt. Because the H_2 atmosphere will contain a certain amount of H_2O, the reaction to be considered is:

$$Be + H_2O \rightarrow BeO + H_2 \qquad (A.3)$$

By the mass action law:

$$K = \frac{p_{H_2}}{p_{H_2O}} \left(\frac{1}{a_{Be}} \right)$$

and $$\log K = \frac{\Delta G^{o}}{2.3RT}$$

where $a_{BeO} = 1$ (solid phase), $a_{Be} = \gamma N$, and N = mole fraction.

The activity coefficient γ is difficult to determine experimentally and therefore it is common to assume the ideal case, $\gamma = 1.0$. Applying these two equations, one can determine the value of the ratio p_{H_2O}/p_{H_2} above which precipitation is possible. Alternately, if one knows the partial pressure ratio in the crystal puller, one can determine the maximum concentration of dopant allowed before precipitation will occur.

Appendix 2

Hall Effect Measurements: Theory and Technique

The equipment for measuring both dark Hall and photo-Hall effect includes a Lakeshore Cryostat (Model CT-310), a 6 kG electromagnet, and an automated electronics and data collection system controlled by an HP-85 computer (54). The samples are mounted on a Cu cold finger, and temperature control is maintained by using a continuous He flow and a resistive heater in conjunction with a temperature sensing feedback diode (Figure A1). Parallelpiped samples measuring 6x6x1 mm^3 were used in the van der Pauw geometry (55). Indium alloyed contacts or B implanted contacts were used for p-type samples.

The expression for tne concentration of free holes as a function of temperature for a two-level system is given by:

$$p = \frac{1}{2}\ (\phi + N_A - N)\left[\left(1 + \frac{4\phi N}{(\phi + N_A - N)^2}\right)^{1/2} - 1\right] \qquad (A2.1)$$

where $N = N_A - N_D$, $\phi = g^{-1} \exp(E_A/kT)$, g is the degeneracy factor, and E_A is the ionization energy of the acceptor level.

Although this simplifies to the well known half-slope and full slope regimes for certain temperature ranges, it is usually necessary to solve the quadratic equation over the entire range of temperature to determine the freeze-out curve.

For a multi-level system, the equation will be a polynomial of n + 1 degree where n is the number of acceptor levels to be considered. For a two level system, this means a cubic equation:

$$p^3 + [\phi_1 + \phi_2 + N_{A1} + N_{A2} - (N_A - N_D)]p^2$$
$$+ [\phi_1\phi_2 + N_{A1}\phi_2 + N_{A2}\phi_1 - (N_A - N_D)\phi_1 - (N_A - N_D)\phi_2]p$$
$$- (N_A - N_D)\phi_1\phi_2 = 0 \qquad \text{(A2.2)}$$

The solution is:

$$p = 2(r^2 + |s|)^{1/6} \cos\left(\frac{1}{3}\right)\left[\tan^{-1}\left(\frac{s}{r}\right)\right] - \frac{a_2}{3} \qquad \text{(A2.3)}$$

where $$q = \frac{1}{3}a_1 - \frac{1}{9}a_2^2 \qquad \text{(A2.4)}$$

$$r = \frac{1}{6}(a_1a_2 - 3a_0) - \frac{1}{27}a_2^3 \qquad \text{(A2.5)}$$

$$|s| = q^3 + r^2 \qquad \text{(A2.6)}$$

for $p^3 + a_2p^2 + a_1p + a_0 = 0$

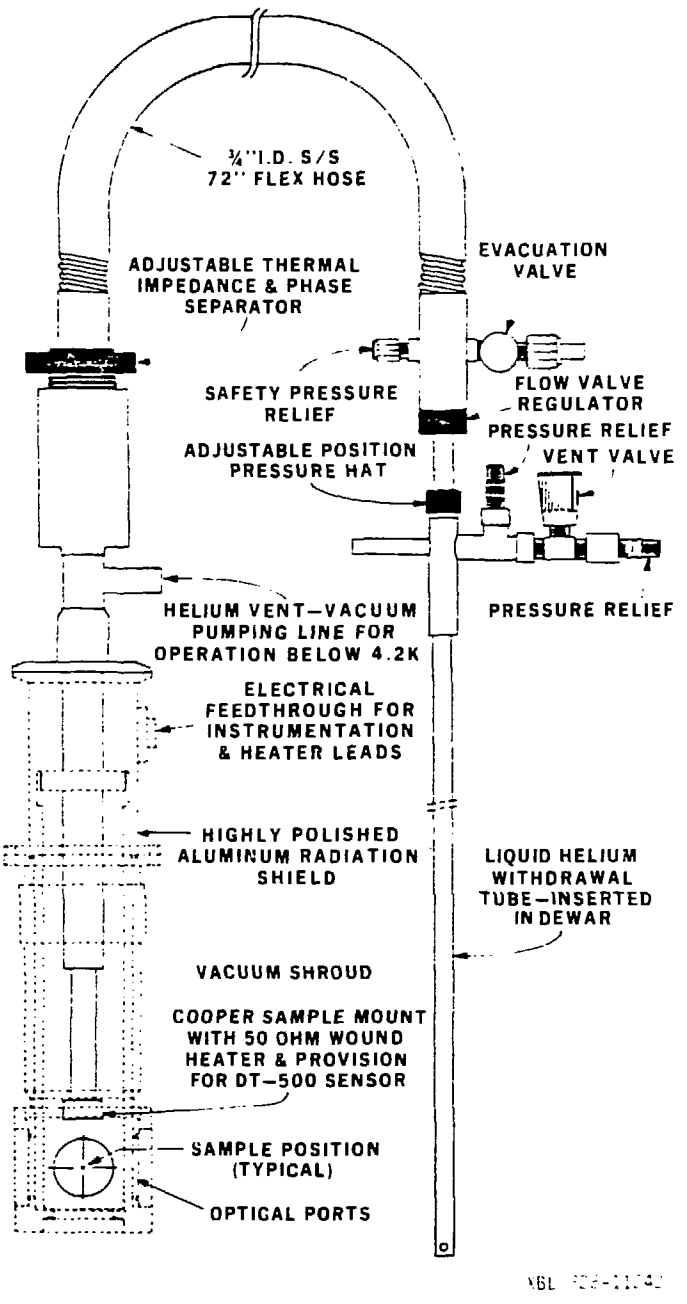

Figure A1
Hall effect measurement apparatus

This report was done with support from the Department of Energy. Any conclusions or opinions expressed in this report represent solely those of the author(s) and not necessarily those of The Regents of the University of California, the Lawrence Berkeley Laboratory or the Department of Energy.

Reference to a company or product name does not imply approval or recommendation of the product by the University of California or the U.S. Department of Energy to the exclusion of others that may be suitable.